ELSEVIER

Journal of Structural Geology 26 (2004) 1561–1589

JOURNAL OF STRUCTURAL GEOLOGY

www.elsevier.com/locate/jsg

The geometry and topology of natural sheath folds: a new tool for structural analysis

G.I. Alsop[a,*], R.E. Holdsworth[b]

[a]*Crustal Geodynamics Group, School of Geography & Geosciences, University of St. Andrews, Fife KY16 9AL, UK*
[b]*Reactivation Research Group, Department of Geological Sciences, University of Durham, Durham DH1 3LE, UK*

Received 15 August 2003; received in revised form 28 January 2004; accepted 29 January 2004

Available online 19 May 2004

Abstract

Curvilinear sheath folds are classically depicted as displaying symmetrical geometries about two orthogonal mirror planes centred along the (X–Y) axial surface and the (X–Z) medial (culmination/depression) surface which bisects the fold nose. However, 10,000 geometric analyses of minor folds and fabrics formed during ductile thrusting in the Caledonides of northern Scotland reveals that major dome and basin sheath folds can display distinct and predictable asymmetries across both axial and medial surfaces. The strain is typically heterogeneous so that structural fabrics and younging evidence are preserved within sheath folds at varying stages of development. This allows an analysis of the evolution of such structures from 'tongue' folds to more extreme 'tubular' forms. Geometric relationships between measured orientations of fold hinges, axial planes, extension lineations and foliations are compared on *fabric topology plots* (FTPs), which provide an effective tool for monitoring planar and linear fabric rotations with increasing progressive non-coaxial deformation. They consistently display systematic variation from regions of lower to higher strain on passing from upper to lower fold limbs across major axial surfaces, and on crossing medial surfaces from short to long hinge-line segments. Axial and medial surfaces effectively therefore divide major sheath folds into quadrants with different amounts, senses and combinations of planar and linear fabric rotation within each domain. Such heterogeneous deformation implies that models of intense non-coaxial deformation *uniformly* affecting pre-existing folds may overestimate bulk displacement and shear strain. Variable fold hinge-line rotation about medial surfaces also provides an effective mechanism for the closure of major sheaths, which may otherwise project for unfeasible distances in the X direction. Bedding/cleavage intersections are developed at greater angles to the transport direction than fold hinges which they transect in a consistent and predictable sense thereby confirming the direction of fold rotation even in areas which lack information on fold facing. In cross-section, asymmetric *tear-drop eyes* indicate the sense of fold hinge-line vergence, whilst fold limb and hinge-line asymmetry may be combined on 3-D vergence, *ranking* and *rotation grids*, which allow location and relative strain states of minor structures to be accurately predicted within the overall sheath framework. Systematic fabric analysis on FTPs may be applied to the investigation of ductile deformation across a broad range of scenarios.

Keywords: Sheath folds; Shear zones; Structural fabrics; Caledonides

1. Introduction

Sheath folds displaying highly curvilinear fold hinge geometries are a widespread phenomenon recognised from high-strain zones within orogenic belts (e.g. Carreras et al., 1977; Quinquis et al., 1978; Minnigh, 1979; Berthé and Brun, 1980; Henderson, 1981) and have also been reported from other settings in which heterogeneous shear occurs, e.g. salt flows and diapirs (Talbot, 1979; Davison et al., 1996; Velaj et al., 1999), glaciers (Hudleston, 1992), deformed sub-glacial sediments (Van der Wateren et al., 2000) and soft sediment slumps (Roberts, 1989). Sheath folds are classically depicted as displaying symmetrical geometries about two orthogonal mirror planes, the (X–Y) axial surface and the (X–Z) medial (culmination/depression) surface which bisects the parabolic fold nose (e.g. Alsop, 1994 and references therein) (Fig. 1). They have been broadly classified by Ramsay and Huber (1987) as folds with a hinge line variation of more than 90°, whilst Skjernaa (1989) further subdivides sheaths

* Corresponding author. Tel.: +44-1334-463937; fax: +44-1334-463949.
E-mail address: gia@st-andrews.ac.uk (G.I. Alsop).

0191-8141/$ - see front matter © 2004 Elsevier Ltd. All rights reserved.
doi:10.1016/j.jsg.2004.01.009

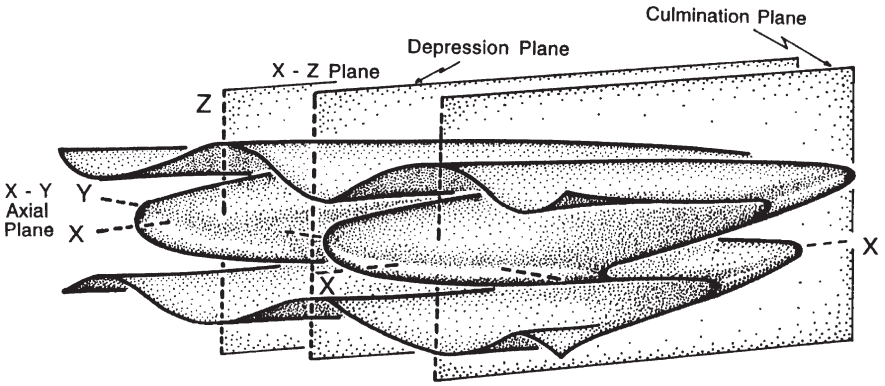

Fig. 1. Schematic 3-D cartoon illustrating the geometric (X–Y–Z) co-ordinates of traditional sheath folds. The sheath folds display horizontal (X–Y) axial planes and vertical (X–Z) medial surfaces separated into culmination and depression planes which close towards and away from the viewer, respectively. See text for further details.

into tubular folds with apical angles of $<20°$. Sheath folds with apical angles of between 90 and 20° may be referred to as *tongue folds* owing to the original description of "a tongue rising steeply in one place" (Carey, 1962, p. 128) and the overall tongue-like morphology of such folds (Fig. 2). These folds typically plot in the non-cylindrical rather than domical field of the PQR diagram (Williams and Chapman, 1979).

Sheath folds are considered to typically form by the rotation of fold hinges that initiate at a high angle to shear during progressive non-coaxial deformation (e.g. Cobbold and Quinquis, 1980). Folds that originally form broadly orthogonal to the transport direction may undergo opposing senses of rotation at either end of their hinge-lines, thus accentuating the gentle primary curvilinearity of the hinge. An originally consistent fold geometry which undergoes

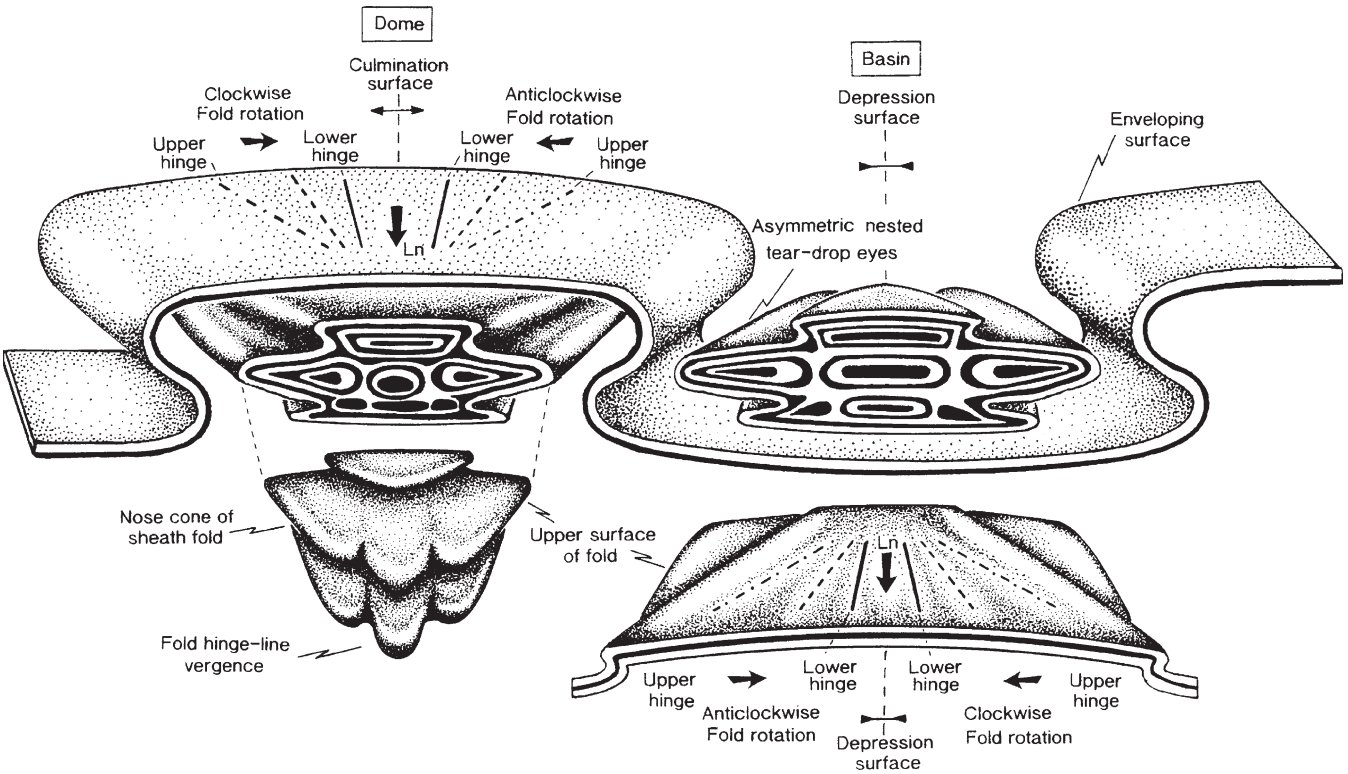

Fig. 2. Schematic 3-D sketch illustrating clockwise and anticlockwise rotation domains around dome and basin sheath geometries. Increasing minor fold rotation from upper to lower limbs is associated with a reduction in fold apical angles from tongue folds to more extreme tubular folds. Variable strain around secondary culmination/depression (medial) surfaces is associated with a systematic variation in fold hinge-line obliquity (about Ln) resulting in fold hinge-line vergence towards major culminations. In cross-sectional view this results in asymmetric nested tear-drop eye folds. General trends of minor folds developed on the upper to lower limbs of the sheath folds are projected (as dashed lines) on the enveloping surface together with the extension lineation (Ln), which parallels the trend of tectonic transport. The sense of clockwise or anticlockwise fold rotation associated with increasing strain from upper to lower fold limb is also illustrated. Refer to text for further details.

clockwise and anticlockwise rotations (viewed on the X–Y plane from above) will thus display mirror image geometries and reversals in minor fold vergence and facing along its hinge length (e.g. Hobbs et al., 1976, p. 168; Holdsworth and Roberts, 1984; Alsop and Holdsworth, 1999; Hanmer and Greene, 2002) (Fig. 2). Sheath folds may also display asymmetric curvilinearity of fold hinges resulting in fold hinge-line vergence (Alsop and Holdsworth, 1999) (Fig. 2). Portions of fold hinge-lines that have rotated in an opposing sense are separated by transport-parallel and foliation-normal medial surfaces that are divided into culminations and depressions (Figs. 1 and 2). Curvilinear folds which are convex up when viewed in the inclined (X–Y) axial surface and closing in the direction of thrust transport are termed culminations, whilst those which are convex down and open in the direction of thrust transport are named depressions (Alsop and Holdsworth, 1999) (Figs. 1 and 2). Culminations and depressions are bisected by foliation-normal and transport-parallel medial surfaces which may intersect both antiformal and synformal axial surfaces. This results in a range of configurations including domes (culmination on antiform) and inverted saddles (culmination on synform), whilst depressions may produce basins (depression on synform) and saddles (depression on antiform) (see Alsop and Holdsworth (1999) for a review) (Fig. 2). Detailed fabric relationships (see below), coupled with the preservation of abundant shear criteria (e.g. Holdsworth, 1989, 1990; Holdsworth et al., 2001) suggest that fold rotation during progressive non-coaxial deformation is the fundamental mechanism of generating sheath folds within the present study.

Thus, this paper develops and builds on earlier observations of sheath folding (Alsop and Holdsworth, 1999) and provides a detailed 3-D analysis of planar and linear fabric patterns and associated rotations around natural examples of major curvilinear fold geometries. This study clearly documents a series of methodologies and observational tools that enable the nature of heterogeneous deformation to be determined, and thereby provides a qualitative guide to combinations of fold and fabric rotations related to strain variations and gradients across both axial and medial surfaces. Geometric analyses of (~10,000) planar and linear fabric relationships, collected from examples of real sheath folds in this case study, provides a statistical consistency in different structural domains within both end-member (domal and basinal) sheath fold frameworks. The remarkable consistency of results allows the techniques presented to act as a predictive methodology thay may have universal application within systems of ductile flow across a range of geological environments.

2. Mapped patterns of sheath folds in the Melness–Sleiteil area

The well exposed areas of detailed study around the Kyle of Tongue, on the north coast of Scotland are composed of probable Late-Archean acidic orthogneisses (Lewisian Complex) which forms a basement to Neoproterozoic psammites and subordinate pelite (Moine Supergroup) which contains weak bedding-parallel S1 fabrics and rare minor F1 folds (see Holdsworth et al., 2001 and references therein). The Melness region to the west of the Kyle of Tongue is dominated by Caledonian (D2) structures which form the focus of the present study, and in particular a ductile thrust stack associated with the Ben Hope Thrust, together with a WNW–ESE-trending major culmination trace. Lewisian orthogneiss carried in the hanging wall of WNW-directed ductile thrusts is often located in the core regions of antiformal closures which dominate this area (Holdsworth, 1990) (Figs. 3–5). To the north of the major culmination trace, secondary medial surfaces with a spacing of ~300 m are offset consistently towards the north in the hanging wall of D2 ductile thrusts (Figs. 5a and 6a and b). This may reflect the slight anticlockwise obliquity between the trend of secondary medial surfaces and the major culmination that is parallel to the thrust transport direction and therefore displays no offset (Figs. 4a and 5a). The offset of secondary medial surfaces by D2 ductile thrusts is consistent with the thrusts forming during continued shearing within an evolving progressive deformation framework (Holdsworth, 1989, 1990; Holdsworth and Grant, 1990).

In detail, the regional foliation (Sn) is a bedding sub-parallel fabric that dips gently towards the east and intensifies into zones of platy mylonite associated with the D2 ductile thrusts (Holdsworth, 1990; Alsop and Holdsworth, 1993). Within the plane of the foliation a well-developed extension lineation (L2) defined by elongate quartz and feldspar aggregates consistently plunges gently towards the ESE, sub-parallel to tight, minor F2 folds of bedding associated with gently east-dipping axial planes marked by the S2 cleavage (Fig. 4). The trend of L2 and the associated foliation (Sn) remain unaffected by subsequent lineation-parallel open folds that plunge gently towards the east (Fig. 4) (Alsop and Holdsworth, 1993, 2002, 2004; Alsop et al., 1996).

The development of major culmination surfaces, coupled with antiformal closures indicates a dominant domal pattern (antiform on culmination) in Melness (Figs. 3–5). Within the adjacent Sleiteil area to the east of the Kyle of Tongue (Fig. 3), the principal arrangement is synformal F2 folds (cored by Moine psammite) and a major depression surface resulting in a dominant basin configuration (Alsop and Holdsworth, 1999) (Fig. 7a–c). Thus, the Melness and Sleiteil areas contain a major culmination and depression surface, respectively, which enable a detailed structural analysis of the two end member scenarios of domal and basinal sheath folding. Secondary culminations and depressions are associated with asymmetric fold hinge-line vergence around both of the major culmination and depression surfaces. The general predominance of south-facing minor F2 folds suggests overall fold hinge-line

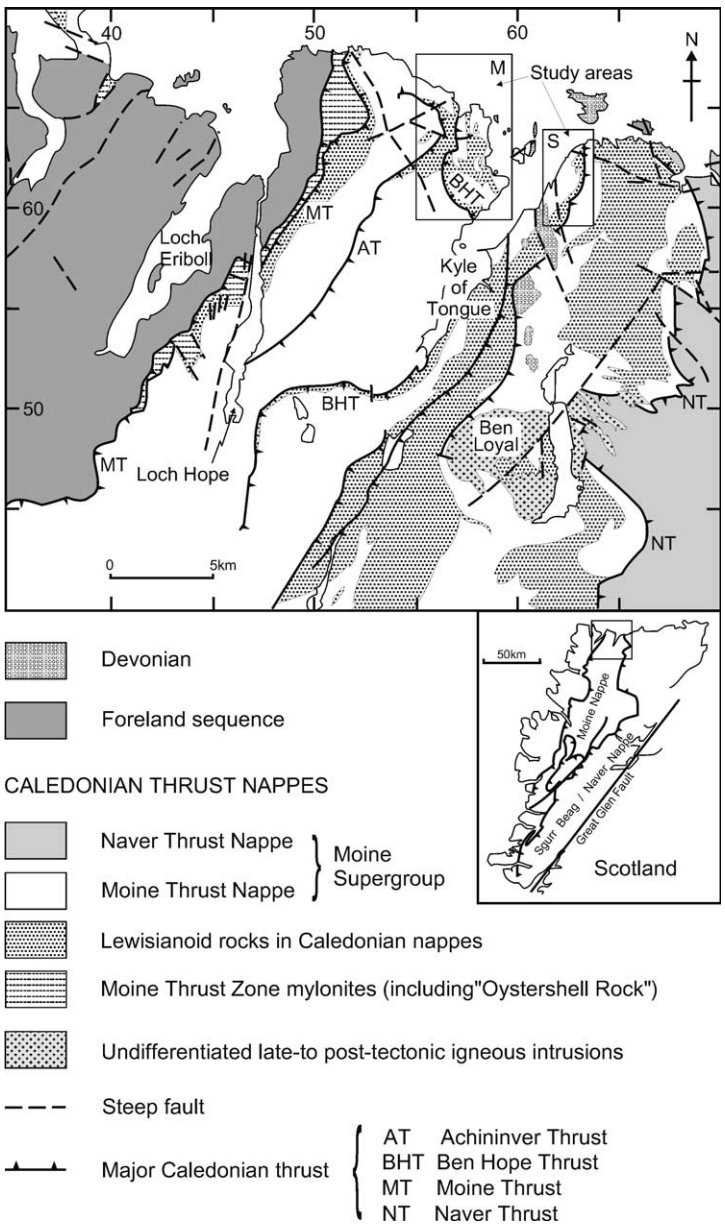

Fig. 3. Simplified geological map of the Moine and Naver Nappes in the Kyle of Tongue area highlighting the location of the Melness (M) and Sleiteil (S) study areas (see also British Geological Survey, 1997, 2002). Major NW-to-WNW-directed Caledonian ductile thrusts that carry reworked Lewisian in the hanging wall are shown with solid barbs. The reference grid relates to the UK National Grid with the map area falling within the NC prefix quadrangle. The inset shows the location of the map in relation to Scotland with the Moine and Naver Nappes being carried on Caledonian thrusts.

vergence towards the north in both Sleiteil and Melness (Alsop and Holdsworth, 1999) (see below).

Theoretical models of sheath folds generated by simple shear demonstrate that folds verging in the direction of shear will develop short limbs which become increasingly attenuated as they rotate towards the shear plane and into the extensional field during continued shear (Skjernaa, 1989; Mies, 1993). Clearly the geometry of the initial folding, and the relative obliquity of the long and short limbs to the shear plane will strongly influence the shape of the resulting sheath fold. However, the typical scenario (and that envisaged in this study) of antiformal buckle folds with short steep limbs dipping in the direction of shear and long limbs sub-parallel to the shear plane will ultimately generate overturned antiforms with attenuated lower limbs (e.g. Fossen and Rykkelid, 1990). In addition, typically upright, open–close synformal buckles will also rotate during simple shear deformation resulting in overturned synforms with attenuated lower limbs (see Mies, 1993; Ez, 2000). The relationships presented in this case study are considered to represent the common situation encountered in evolving systems of progressive deformation where original buckle folds initiate at a high angle to shear and, verging in the direction of transport, are subsequently modified by continued shearing within the same overall kinematic framework.

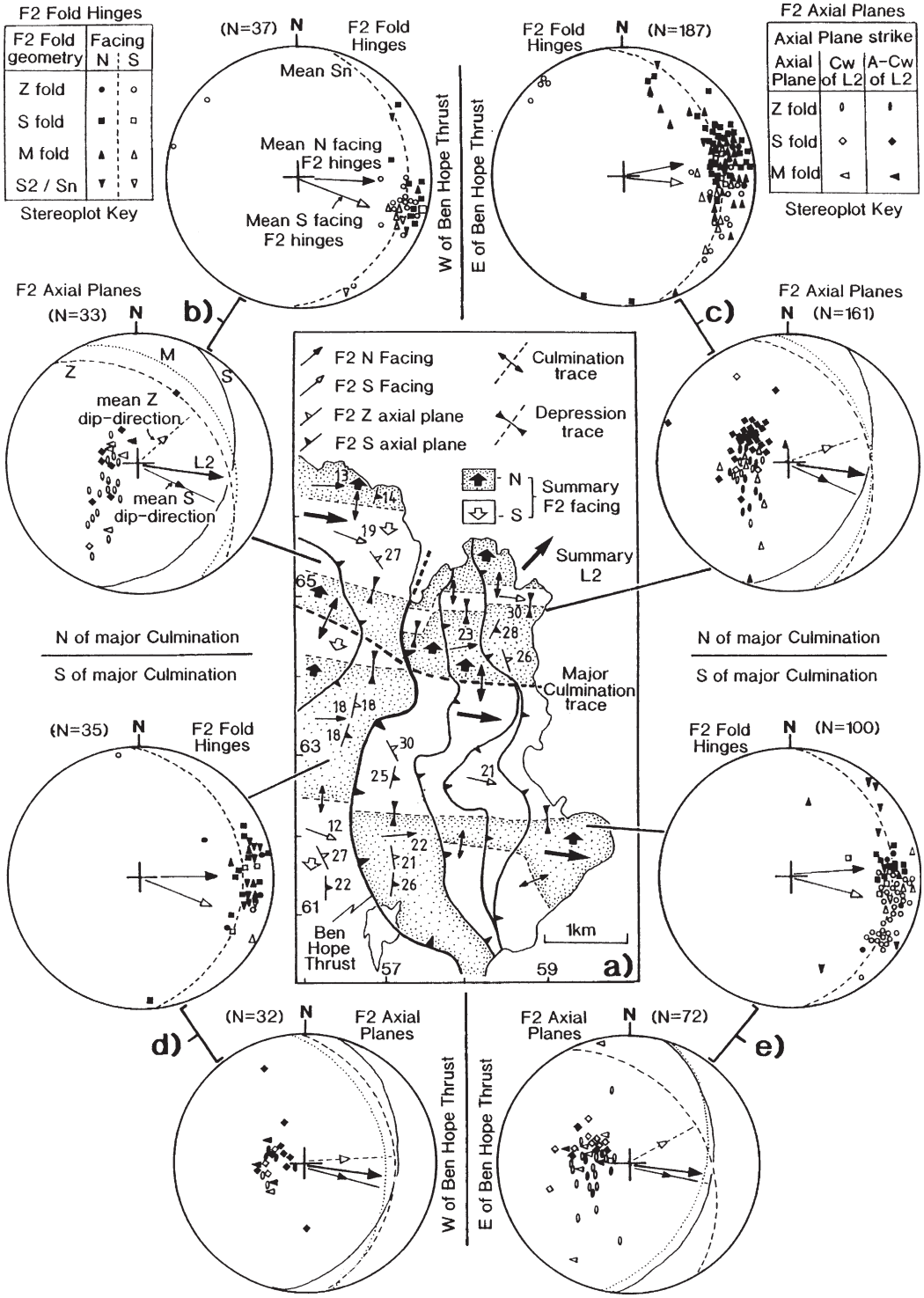

Fig. 4. Simplified structural map of the Melness area highlighting the location of the ductile Ben Hope Thrust, and a major ~W–E-trending culmination trace, which together divide the region into four structural sub-areas. Equal area lower hemisphere stereographic projections of poles to F2 axial planes, together with F2 fold hinges collected relative to this culmination and thrust are also shown. Summary facing domains (based on younging evidence) are highlighted in stipple. Note that the intersection of the great circles representing the mean Z and S axial planes is typically parallel to the extension lineation (L2). D2 measurements in each subarea of the map represent mean data for each domain, with solid and open symbols representing north- and south-facing structures, respectively. Refer to Fig. 3 for location.

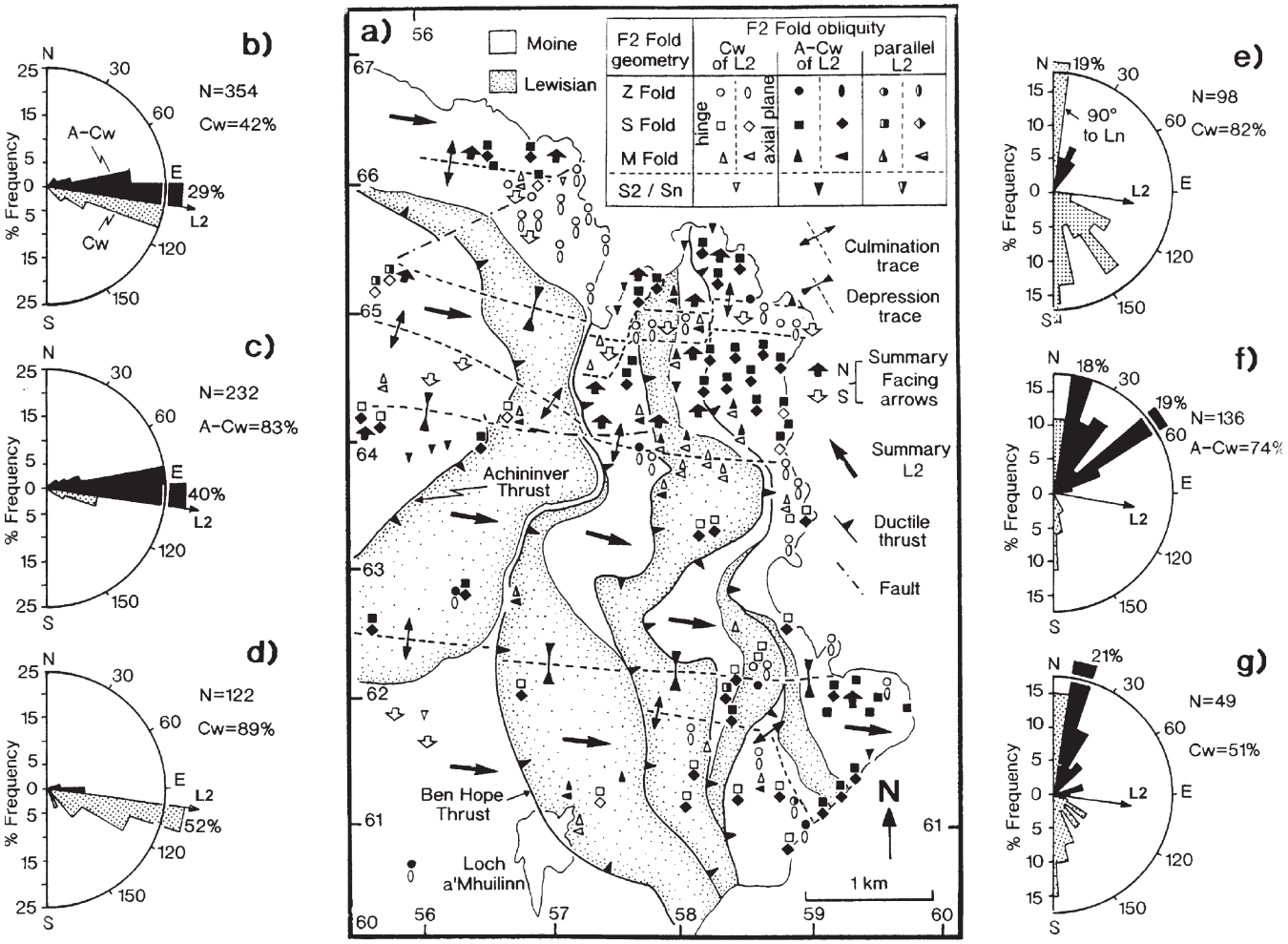

Fig. 5. (a) Detailed map of structural analysis within Lewisian and Moine rocks of the Melness area illustrating the vergence and facing relationships of minor F2 folds, together with the relative obliquity between F2 hinges and the L2 extension lineation. Fold hinge obliquity of (b) all minor F2 folds, (c) north-facing F2 folds and (d) south-facing F2 folds is measured relative to the adjacent extension lineation (L2) and is described as clockwise (Cw) (open symbols and stipple) or anticlockwise (A-Cw) (solid symbols). A consistent (~86%) relationship exists between the direction of fold facing and sense of obliquity of minor F2 hinges. The strike of F2 axial planes is measured relative to the trend of the L2 extension lineation for (e) F2 Z fold axial planes, (f) F2 S fold axial planes and (g) F2 M fold axial planes. Z fold axial planes are typically (mean = 60°) clockwise and S fold axial planes typically (mean = 74°) anticlockwise of L2. Refer to Fig. 3 for location and text for further details.

3. Fabric relationships associated with sheath folding

Within ductile deformed rocks, a variety of simple structural relationships associated with obliquities between planar and linear fabrics may be measured. Such an approach enables a greater understanding of both the geometric consequences of deformation, and the tectonic evolution of the deforming system. The rationale of this geometric analysis is based on the concept of fabric attractors (Passchier and Trouw, 1996, p. 19; Passchier, 1997) with increasingly higher strains resulting in planar and linear fabric rotation towards the shear plane and X direction (respectively) (e.g. Ramsay, 1960, 1967, 1980; Escher and Watterson, 1974; Ramsay and Huber, 1987, p. 595; Ramsay and Lisle, 2000, p. 968). Within zones of intense simple shear ($\gamma = 10$), extension lineations (Ln) will be sub-parallel (~5°) to the movement direction. Thus, with increasing non-coaxial deformation, fold hinges rotate towards the extension lineation (e.g. Escher and Watterson, 1974; Rhodes and Gayer, 1977; Williams, 1978; Mies, 1991), whilst axial surfaces rotate towards sub-parallelism with the main foliation (e.g. Sanderson, 1973; Escher and Watterson, 1974; Carreras et al., 1977; Bell, 1978; Cobbold and Quinquis, 1980; Fossen and Rykkelid, 1990; Alsop, 1992). Given the relationships noted above, we consistently use the trend of the extension lineation (Ln) and strike of the foliation surface (Sn) as the reference datum about which the relative obliquity of the various fabric elements are measured. We shall now examine the various structural geometries associated with D2 sheath folding in more detail, with each section being introduced by a positive (italicised) statement that highlights the structural relationship under discussion.

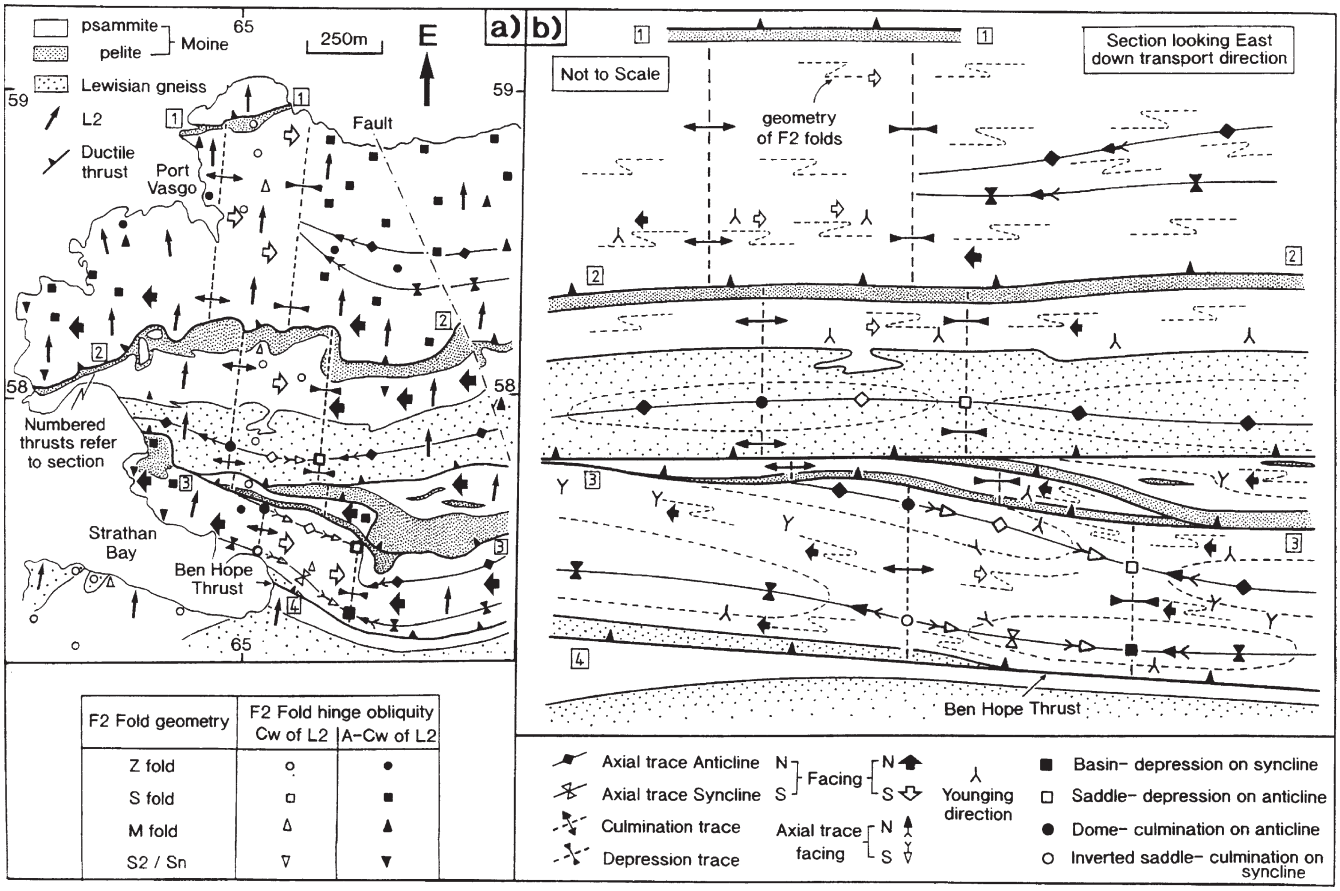

Fig. 6. Detailed map (a) and transport-normal section (b) of the area to the north of the major culmination and east of the Ben Hope Thrust (refer to Figs. 3 and 4). The map and section illustrate the vergence and facing relationships of minor F2 folds, together with the relative obliquity between F2 hinges and the L2 extension lineation. Fold hinge obliquity of minor F2 folds is measured relative to the adjacent L2 and is described as clockwise (Cw) (open symbols) or anticlockwise (A-Cw) (solid symbols). A consistent (~87%) relationship exists between the direction of fold facing and sense of obliquity of minor F2 hinges. When viewed down-plunge, secondary culmination and depression surfaces are offset in a consistent sinistral (top-to-the-north) sense by D2 ductile thrusts (labelled 1–4) located along pelitic units, suggesting strain localisation and continued progressive deformation within these weaker horizons.

3.1. Minor fold geometry

The sense of minor fold vergence will display distinct reversals on crossing both major axial and medial surfaces. Minor folds typically display predictable patterns of long limb–short limb asymmetry or vergence about associated major folds (Bell, 1981). When viewed down fold–plunge such vergence relationships may conveniently be described as Z-, S- or neutral-verging M/W fold geometries. Minor folds display reversals in asymmetry *across-strike* when crossing major fold axial traces (e.g. Figs. 6a and b and 7a and b). However, in regions of curvilinear folding, reversals in vergence will also occur *along-strike* when medial (culmination/depression) surfaces are crossed (see Alsop and Holdsworth, 1999). Within both Melness and Sleiteil, reversals in minor fold vergence clearly occur across both major fold axial surfaces and medial surfaces (Figs. 5a, 6a and b and 7a and b). Thus, the position of a minor fold on a major sheath fold is not uniquely located by analysis of asymmetry alone. Additional discriminatory information is therefore required and is provided by the study of minor fold facing patterns.

3.2. Minor fold facing

The sense of minor fold facing will display distinct reversals in polarity only on crossing medial surfaces which typically define the trend of tectonic transport. Fold facing is defined as "the direction, normal to the fold hinge, along the fold axial plane, and towards the younger beds" (see Holdsworth, 1988). Moine psammites locally preserve sedimentary structures such as graded bedding and cross bedding, which enable the 'way-up' to be determined and hence the sense of minor fold facing. F2 fold hinges in both Melness and Sleiteil define stereographic girdle patterns over arcs of 180° (Figs. 4b–e and 7d–f). Such arcs and associated best-fit great circles striking normal to transport (X) (i.e. parallel the Y axis of the bulk finite strain ellipsoid) indicate that sheaths originated as NNE-trending buckles which overturned towards the WNW prior to modification

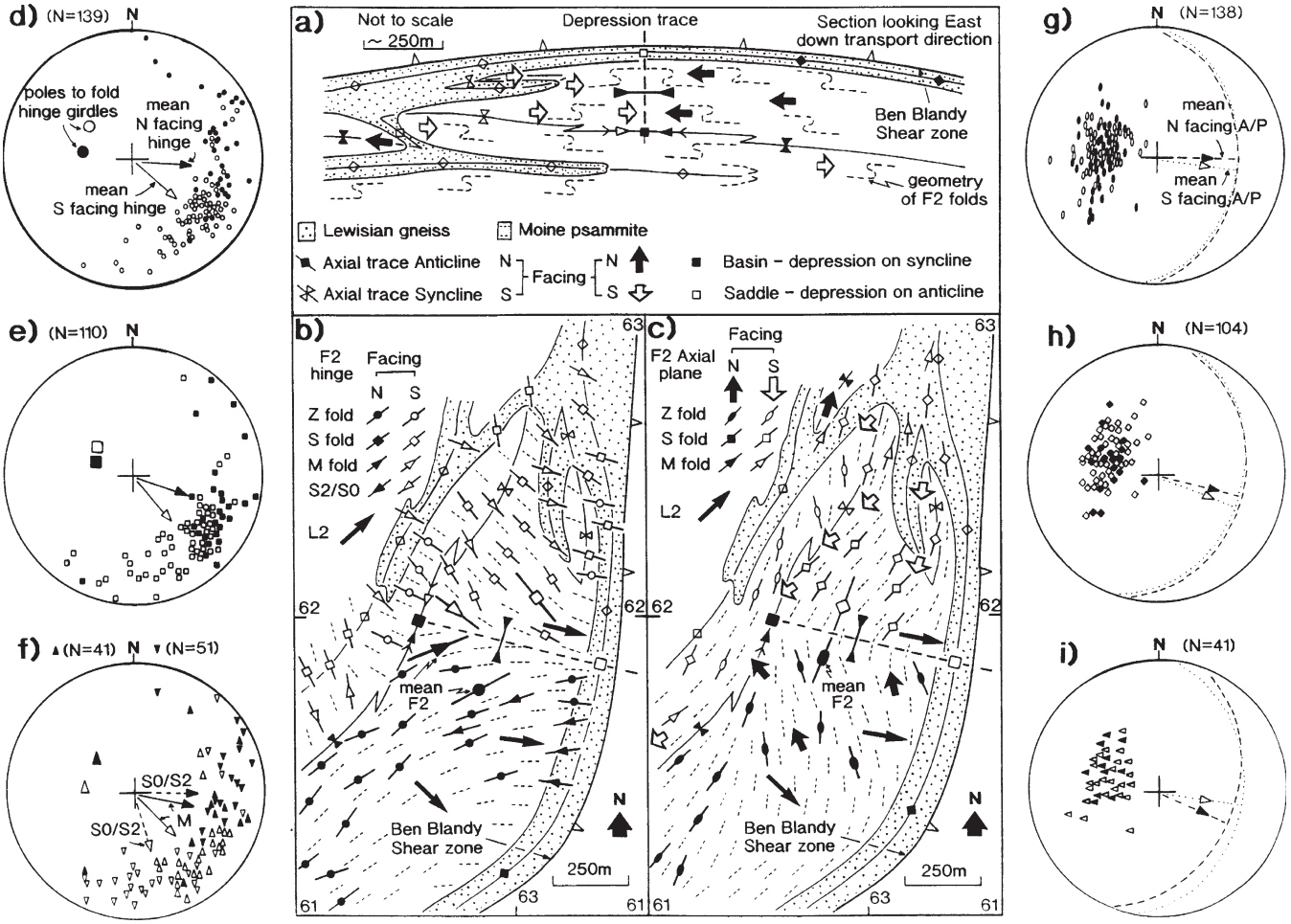

Fig. 7. Transport-normal section (a) and F2 fold hinge (b) and axial plane (c) maps of the Sleiteil area. Refer to Fig. 3 for location. The maps and section illustrate the vergence and facing relationships of minor F2 folds, together with the relative obliquity between F2 hinges and the L2 extension lineation. Fold hinges and associated axial planes are described as north-facing (closed symbols) or south-facing (open symbols) and typically display anticlockwise (93%) and clockwise (90%) relationships to the adjacent L2 extension lineation (respectively). Note how minor folds define an overall divergent pattern and rotate towards L2 in regions of greater strain adjacent to the depression trace, the lower synformal fold limb and also the Ben Blandy shear zone. In general, north-facing fold hinges are more oblique to the trend of L2 as they are located on the regional (lower strain) short hinge-line segment. F2 axial planes on the upper synformal limb display an overall synformal warp. A consistent (~88%) relationship exists between the direction of fold facing and sense of obliquity of minor F2 hinges. North-facing (closed symbols) and south-facing (open symbols) F2 fold hinges are shown for (d) F2 Z folds, (e) F2 S folds and (f) F2 M folds (▲) and S0/S2 intersections (▼). Poles to best fit fold hinge girdles associated with north- and south-fold facing are presented in each case, with differing poles reflecting opposing (clockwise and anticlockwise) rotation paths. North-facing (closed symbols) and south-facing (open symbols) F2 fold axial planes for (g) F2 Z axial planes, (h) F2 S axial planes and (i) F2 M axial planes are also given.

and rotation during D2 shear (Holdsworth, 1988, 1989, 1990). Minor fold facing patterns will display similar variability, with the polarity of facing dependent on the sense of minor fold hinge rotation. As minor fold hinges are generally east-plunging sub-parallel to L2, associated fold facing may be divided into broadly north- or south-facing polarity. Culmination and depression surfaces marked by along-strike reversals in minor fold vergence are also therefore associated with reversals in the polarity of minor fold facing to define north- and south-facing domains (Figs. 4a, 5a, 6a and b and 7a–c). Thus, facing azimuths are directed inwards towards depression surfaces and outwards away from culmination surfaces (Alsop and Holdsworth, 1999).

Within the Sleiteil area, best fit great circles to south-facing S and Z fold hinge girdles strike clockwise compared with their north-facing equivalents which are more orthogonal to L2 (Fig. 7d and e). Neutral-verging M folds do not display this pattern as they are not uniquely located with respect to the upper or lower limbs in the overall sheath fold (Fig. 7f). This relationship reflects the location of north-facing folds on regional short hinge-line segments (see Section 2), and rotation paths of opposing sense between north- and south-facing fold domains. The orientation of minor fold axial planes is variable, with the dip direction of south-facing Z fold axial planes and north-facing S fold axial planes being most parallel to L2 (Fig. 7g–i). This is a consequence of these minor folds being located on (more highly strained) lower fold limbs in Sleiteil, i.e. the dip direction of minor axial planes rotates towards the transport direction with increasing dip-slip deformation

(see Section 4). Thus, on stereographic projections, the trend of tectonic transport will therefore be defined (irrespective of lineations) by the acute bisector separating reversals in polarity of fold facing.

3.3. Minor fold hinge/extension lineation obliquity

The sense of minor fold hinge/extension lineation obliquity will display distinct reversals on crossing medial surfaces. The angular obliquity between the trend of a fold hinge relative to the extension lineation (datum) may be described as clockwise or anticlockwise when viewed on the axial (X–Y) surface from above. Within regions of heterogeneous shear, increasingly large shear strains are required to drive complete rotation of fold hinges into parallelism with the extension (X) direction (Skjernaa, 1980). Consequently, precise co-linearity between fold hinges and extension lineations is rarely achieved and small but distinguishable angles of obliquity are commonly preserved. Minor folds that rotate in an opposing sense towards the transport direction will therefore display an opposing sense (clockwise or anticlockwise) of fold hinge/extension lineation obliquity. Reversals in the sense of this obliquity about the extension lineation (datum) will develop with along-strike reversals in minor fold vergence and facing polarity and mark the medial surfaces (Alsop and Holdsworth, 1999). 87% of north-facing folds preserve an anticlockwise obliquity whilst south-facing folds are consistently (90%) clockwise of the extension lineation (Figs. 5a–d and 6a and b). Regions of north-facing minor folds associated with anticlockwise obliquities are developed north of culmination traces whilst south-facing folds clockwise of the lineation are mapped to the south of culminations thus defining an overall convergent fold trace pattern in the transport direction (Figs. 4a–e, 5a and 6a). The converse is true around depressions where fold trace patterns diverge in the transport direction (Fig. 7b). Thus, the sense of hinge/extension lineation obliquity will display distinct reversals on crossing medial surfaces. However, the sense of obliquity within any facing domain always remains the same—no matter what the fold hinge geometry and relative position to large-scale axial surfaces.

3.4. Minor fold axial plane/extension lineation obliquity

The sense of minor fold axial planar strike/extension lineation obliquity will display distinct reversals on crossing both major axial surfaces and medial surfaces. The angular obliquity between the strike of a fold axial plane relative to the trend of the extension lineation (datum) may be described as clockwise or anticlockwise when viewed from above. Whilst obliquity of fold hinges to L2 is dependent on the direction of fold facing, the obliquity of fold axial planes is governed by fold geometry and is not dependent on facing. This is a consequence of Z and S axial planes dipping towards and converging around dome and basin configurations, with the variation in strike reflecting the gently-dipping ($\sim 20^\circ$) nature of the dip-slip system. When compared with the trend of the extension lineation (L2), the strike of minor Z fold axial planes is typically (82%) clockwise of L2, whilst S fold axial planes are normally (74%) anticlockwise. Minor inconsistencies largely reflect axial planes which strike broadly orthogonal to L2, but which have passed marginally through the transport-normal into the opposing field of obliquity (Fig. 5e–g). As may be anticipated, neutral verging M fold axial planes do not display distinct obliquities to L2 (51% clockwise) (Fig. 5e–g).

Axial planar traces of minor folds define an overall synformal pattern across the depression surface in Sleiteil, with axial traces converging towards basin intersections (depression on synforms) and diverging from associated saddles (depression on antiforms) (Fig. 7c). Thus, overall geometry dictates that minor fold axial planes define convergent traces towards end-member basins and domes, and divergent traces around the intermediate saddles and inverted saddles, respectively. Such patterns are most clearly observed in lower strain settings such as the upper limbs of sheath folds (see Section 4 below). North of the major culmination trace in Melness, mean S and Z axial planes display greater obliquity in strike and are bisected by M fold axial planes (compare Fig. 4b and c with Fig. 4d and e). This may reflect their location on a regional short hinge-line segment possibly associated with lesser rotations (see Section 5). Both S and Z axial planes display bimodal peaks at 40–50° and 80–90° from L2 in an anticlockwise and clockwise sense, respectively (Fig. 5e and f). The more orthogonal peaks correspond to data from lower fold limbs, whilst oblique (40–50°) peaks reflect data from upper (lower strain) limbs. A consequence of S and Z fold axial planes striking in an anticlockwise and clockwise sense (respectively) about the L2 trend is that the intersection of the stereographic great circles representing the mean S and Z axial planes is parallel to the direction of tectonic transport (Fig. 4b–e). Such relationships are also recorded in the later flow perturbation folds observed in the region (Alsop and Holdsworth, 2002), and are obviously of value in determining the trend of tectonic transport where lineations are absent or ambiguous.

3.5. Minor fold axial plane/foliation obliquity

The sense of minor fold axial planar strike/foliation obliquity will display distinct reversals on crossing both major axial surfaces and medial surfaces. As exact colinearity of fold hinges with lineations is difficult to achieve (see above), so fold axial planes and foliations marking the dominant (long) fold limbs are also rarely co-planar. Minor folds within the study area typically display tight geometries and associated axial planes are oblique to foliation surfaces (Sn) that mark the fold limbs. The angular obliquity between the strike of a fold axial

plane relative to the strike of Sn (datum) may be described as clockwise or anticlockwise when viewed from above. S fold axial planes are 85% clockwise of Sn strike whilst Z fold axial planes are 92% anticlockwise of Sn strike (Figs. 4a–e and 7g and h). Thus, the sense of axial plane/Sn obliquity for S and Z folds always remains fixed and is therefore independent of both facing and structural position on larger folds. However, as the geometry of minor folds switches on crossing both major axial surfaces and medial surfaces, the sense of axial plane/foliation obliquity observed in each domain will also reverse accordingly.

3.6. Summary

Minor fold hinges and axial planes display differing degrees of rotation relative to datum as defined by the L2 trend and Sn strike, respectively. Whilst no simple planes of symmetry necessarily exist in major sheath folds, two important geometric parameters remain fixed. Firstly, the sense of hinge/extension lineation obliquity for facing domains always remains the same both on the upper and lower limbs of major folds. Secondly, the sense of axial plane/foliation obliquity for S and Z folds always remains fixed—no matter what the position relative to medial surfaces or large-scale axial surfaces.

4. Geometric elements of deformation and sheath folding

Having described the general characteristics of minor structures associated with sheath folding, we now consider in greater detail the inter-relationships between these various factors. A suite of structural parameters are established, which collectively relate to variations in structural position (and hence strain) on larger-scale sheath folds.

4.1. Fabric topology plots—a new structural tool

Topology refers to the invariant properties of a figure under deformation, and may be applied to the study of fold and fabric patterns by defining a series of structural parameters that maintain a constant relationship during deformation. Seven such topological parameters are defined here, which collectively undergo progressive and predictable modification from regions of lower to higher strain (Fig. 8). Detailed analyses of such systematic patterns are presented on traditional frequency distribution histograms (Fig. 9) and also on *fabric topology plots* (FTPs) (Fig. 10). Any two parameters may be directly compared and contrasted with one another on FTPs, which effectively monitor fabric relationships and evolution, and thereby enable a clearer understanding of deformation behaviour (Figs. 8 and 10). FTPs may thus be used to directly compare the typical structural field recordings of fold vergence and facing, together with measurements of the fold hinge, axial plane, extension lineation and foliation orientations making this technique simple, effective and easy to apply. The statistical consistency of our dataset developed from natural sheath folds suggests that a predictive methodology can be confidently applied in areas with poor exposure and/or fewer data. In addition, such techniques may be applied to all terranes in which heterogeneous deformation results in the rotation of planar and linear structural elements towards the fabric attractor (Passchier, 1997).

The various structural associations and their relationships to increasing deformation from lower (designated −ve) to higher (designated +ve) strains in each case are illustrated in Fig. 8. Note that as the reference frame of the parameters frequently refers to variations about a horizontal datum, e.g. extension lineation trends and foliation strike, they are best suited to dip-slip dominated systems of deformation, although conversion into angles of plunge and pitch in sub-vertical strike-slip dominated systems is clearly possible. The angles of hinge and lineation pitch are extremely valuable in steeply dipping axial planes where fold rotations may produce little change in hinge trend. Following convention, values of pitch (rake) are calculated from the horizontal strike and within the plane of the axial surface in each case, whilst the trend of the extension lineation (Ln) and strike of the foliation (Sn) form the reference datum for calculating relative obliquities. The section below provides a commentary on structural relationships summarised in Table 1 and Fig. 8, and presented on FTPs (Fig. 10) to which the reader is referred for further details.

4.2. Fabric topology plots and sheath folding

Within the dome-dominated setting of Melness, south-facing Z fold hinges and north-facing S fold hinges are located on the upper limbs of major antiformal sheaths and, respectively, define 90° clockwise and anticlockwise arcs about L2 (Table 1a; Figs. 8a and 9b and c). Conversely, north-facing Z fold hinges and south-facing S fold hinges are developed on the lower limbs of sheaths and display distinct anticlockwise and clockwise clusters (respectively) within 20° of L2 (Fig. 9a–c). Similar obliquities are also recorded in Sleiteil where 93% of north-facing folds are anticlockwise of L2, whilst south-facing folds are typically (90%) clockwise of the L2 trend. The sense of F2 hinge pitch is directly linked to the strike of the associated Z or S axial plane (Table 1b; Figs. 8b and 10a and e). Within Melness, minor folds from the lower limbs of sheaths display consistently greater values of hinge pitch compared with folds on the upper limbs (Figs. 10a and 11a and c). Data from the basin-dominated Sleiteil area displays a similar pattern with F2 pitch being greatest to the north of the major depression surface on the long hinge-line segment (Figs. 10e and 11f and h). The sense of L2 pitch is also directly linked to the strike of the associated Z or S axial

plane (Table 1c; Figs. 8c and 10b and f). Greater values of L2 pitch are recorded on the lower limbs of domal sheaths (Melness) (Figs. 10b and 11a and d), and also long hinge-line segments (Sleiteil) (Figs. 10f and 11f and i). Within both dome- and basin-dominated settings, the sense of anticlockwise or clockwise obliquity between the pitch of a fold hinge and lineation (datum) is dependent on north- or south-facing (respectively) (Table 1d; Figs. 8d and 10c, g, k and o). Minor fold hinges from the lower limbs of domal sheaths (Melness) (Figs. 10c and l and 11a and d), or long hinge-line segments (Sleiteil) (Figs. 10g and p and 11f and i) display smaller angles of obliquity to L2.

A reversal in the sense of axial planar strike about the extension lineation is a geometrical necessity of folds displaying opposing vergence within non-isoclinal, curvilinear fold systems (Section 3.4). Both S and Z axial planes display bimodal peaks at 40–50° and 80–90° from L2 in a anticlockwise and clockwise sense, respectively (Table 1e; Figs. 8e and 9e–g). The more orthogonal peaks correspond to data from lower fold limbs, whilst oblique peaks reflect data from upper limbs (Fig. 9e). Neutral verging M fold axial planes are symmetrically distributed about L2 (Fig. 9h). The sense of obliquity between axial planar strike and the adjacent foliation (Sn) trend marking the long limb of the fold is also dependent on Z or S fold geometry and is irrespective of the sense of fold facing (see Section 3.5) (Table 1f; Figs. 8f, 10d and h and 12c). The axial planes of minor folds on the lower limb (Melness) and long hinge line segment (Sleiteil) of major sheath folds display smaller differences in trends relative to foliation strike (Fig. 11a, e, f and j). The acute angle between axial planes and long-limb foliation is typically $<20°$ with the sense of obliquity controlled by Z or S fold geometry (Table 1g; Figs. 8g and 9i–k and m–o). Folds from the lower domal limb (Melness) and long hinge-line segment (Sleiteil) typically display more acute angles, whilst M folds are more evenly distributed (Fig. 9l and p).

4.3. Summary

Topological relationships associated with the *sense* of obliquity are governed by the fact that S and Z axial planes are typically NE- and SE-striking, respectively, resulting in associated east-trending fold hinges and extension lineations pitching with a clockwise and anticlockwise sense relative to the axial planar strike. Variable trends of S and Z axial planes also accounts for their respective clockwise and anticlockwise obliquity relative to the ~N–S striking foliation (Sn). Obliquities between trends (or pitch values) of fold hinges and extension lineations (representing datum) are controlled by the sense of hinge rotation with north-facing hinges displaying anticlockwise obliquities, whilst south-facing hinges are clockwise of the extension lineation (see Table 1).

Topological relationships associated with the *amount* of obliquity are governed by the fact that the lower limbs and long hinge-line segments of major sheath folds are marked by (a) smaller angles between fold hinges and extension lineations, greater values of (b) hinge and (c) extension lineation pitch, (d) smaller angles of pitch between fold hinges and extension lineations, (e) greater angles between the strike of axial planes and the extension lineation, (f) smaller differences in trend between axial planar and foliation strike, and (g) reduced acute dihedral angles between axial planes and foliation. These relationships are directly compared in Fig. 11, where mean measurements from upper and lower limbs in Melness (Fig. 11a–e), together with short and long hinge-line segments in Sleiteil (Fig. 11f–j) are especially highlighted. We interpret all of these relationships to be related to increasing strain from the upper to lower limbs, and from the short to long hinge-lines, of major sheath folds (Table 1; Fig. 8).

5. Geometric interplay between medial and axial surface grids

The preceding section has clearly demonstrated that planar and linear fabrics undergo ordered and sequential rotation and modification during deformation. In summary, the sense of obliquity between fold hinges and the lineation relates to the sense of fold facing, whilst the sense of obliquity between axial planar strike and L2 trend or Sn strike is dependent on Z or S fold geometry. FTPs displaying these parameters may thus be divided into quartiles on this basis, e.g. Fig. 10i, j, m and n, and are now explored in more detail via the application of geometric grids that effectively divide sheath folds into four separate analytical domains or quadrants.

5.1. Vergence grids

Reversals in both fold hinge-line and fold limb vergence across medial and axial surfaces effectively divide sheath folds into 3-D asymmetric quadrants as analysed on vergence grids. Fold limb vergence is typically described using S, Z and M terminology (when viewed down the fold plunge). Fold hinge-line vergence may also be described using this classification when viewed on the X–Y surface from above. It is possible therefore to define 3-D fold vergence around both axial and medial surfaces by combining both hinge and limb asymmetry on a vergence grid (Fig. 12a). Such a grid illustrates the range of possible configurations and demonstrates that fold limb and hinge-line vergence are typically the same (i.e. Z on Z, etc.) on the upper limbs of domes and become opposite to one another (i.e. Z on S, etc.) on the lower fold limbs. Conversely, the lower limbs of basins are marked by identical fold limb and fold hinge-line vergence, which reverses on the upper limb (Fig. 12a). Within both the dome and basin setting, the upper limb typically displays lower relative strain (−ve), whilst lower fold limbs undergo greater (+ve) strain.

Topological Parameter Lower Strain (−ve) / Higher Strain (+ve)	Topological Relationship for dip-slip shear system	Amount of Obliquity	Sense of Obliquity	Summary	Figure Ref.
Angle between trend of fold hinge and lineation a) 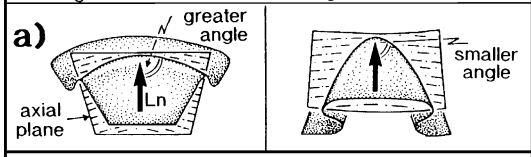	*With increasing shear strain, the acute angle between the trend of a fold hinge and the adjacent extension lineation (X) will reduce as the fold hinge rotates towards the transport direction.*	**Greater angles -** Upper limbs / short hinge-lines **Smaller angles -** Lower limbs / long hinge-lines	**Cw angles -** S facing fold hinges **A-Cw angles -** N facing fold hinges	*The **sense** of obliquity between a fold hinge and lineation is controlled by the direction of hinge rotation, whilst the **amount** of obliquity will reduce as the fold hinge rotates towards the transport direction with increasing deformation.*	Figures 9a,b,c,d, 10i,j,m,n, 11a,b, 12c, Tables 1a,4a
Angle of pitch of fold hinge on axial plane b) 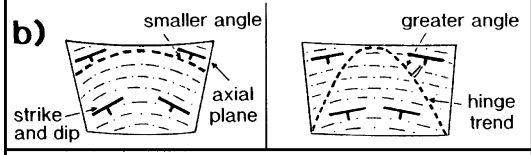	*With increasing shear strain, the angle of fold hinge pitch will increase as the fold hinge rotates towards the down-dip (i.e. pitching 90°) transport direction.*	**Smaller angles -** Upper limbs / short hinge-lines **Greater angles -** Lower limbs / long hinge-lines	**Cw angles -** S fold axial planes **A-Cw angles -** Z fold axial planes	*The **sense** of fold hinge pitch is controlled by the axial planar strike related to Z and S fold geometries, whilst the **amount** of pitch increases as the fold hinge rotates towards the down-dip transport direction with increasing deformation.*	Figures 10a,e, 11a,c,f,h, Tables 1b,4b
Angle of pitch of lineation on axial plane c) 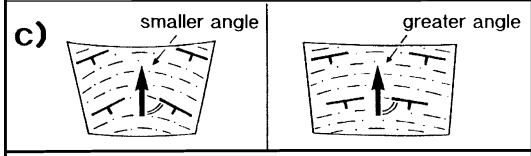	*With increasing shear strain, the angle of pitch of a lineation will increase as the associated fold axial plane rotates towards the shear plane.*	**Smaller angles -** Upper limbs / short hinge-lines **Greater angles -** Lower limbs / long hinge-lines	**Cw angles -** S fold axial planes **A-Cw angles -** Z fold axial planes	*The **sense** of lineation pitch is controlled by the axial planar strike related to Z and S fold geometries, whilst the **amount** of pitch increases as axial planar strike rotates towards the shear plane with increasing deformation.*	Figures 10 b,f, 11a,d,f,i, Tables 1c,4c
Angle between pitch of fold hinge and lineation d) 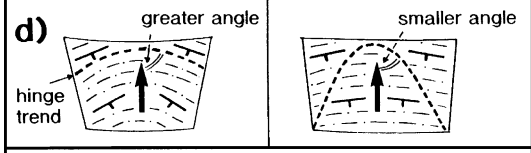	*With increasing shear strain, the angle between the pitch of a fold hinge and lineation will reduce as the fold hinge rotates towards the transport lineation.*	**Greater angles -** Upper limbs / short hinge-lines **Smaller angles -** Lower limbs / long hinge-lines	**Cw angles -** S facing fold hinges **A-Cw angles -** N facing fold hinges	*The **sense** of obliquity between the fold hinge and lineation pitch is controlled by the direction of hinge rotation, whilst the **amount** of obliquity will reduce as the fold hinge rotates towards the transport direction with increasing deformation.*	Figures 10 c,g,k,l, 10 o,p, 11a,d,f,i, Tables 1d,4d
Angle between axial planar strike and lineation trend e) 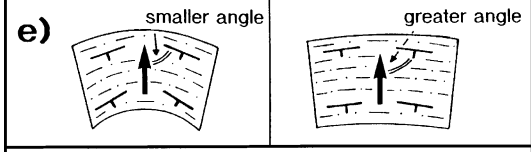	*With increasing shear strain, the angle between axial planar strike and the trend of the extension lineation will increase as the fold axial plane rotates towards the shear plane.*	**Smaller angles -** Upper limbs / short hinge-lines **Greater angles -** Lower limbs / long hinge-lines	**Cw angles -** Z fold axial planes **A-Cw angles -** S fold axial planes	*The **sense** of obliquity between the axial planar strike and the lineation is controlled by Z or S fold geometry, whilst the **amount** of obliquity will increase as the axial plane rotates towards the shear plane with increasing deformation.*	Figures 9 e,f,g,h, 10j,n, 12c, Tables 1e,4e
Angle between strike of axial plane and foliation (Sn) f) 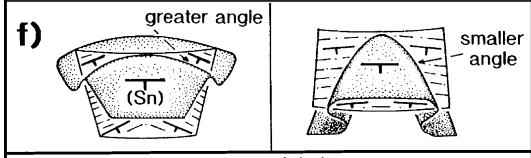	*With increasing shear strain, the angle between the fold axial planar strike and the trend of the adjacent foliation will reduce as the axial plane rotates towards the shear plane.*	**Greater angles -** Upper limbs / short hinge-lines **Smaller angles -** Lower limbs / long hinge-lines	**Cw angles -** S fold axial planes **A-Cw angles -** Z fold axial planes	*The **sense** of obliquity between the axial planar strike and the foliation trend is controlled by Z or S fold geometry, whilst the **amount** of obliquity will decrease as the axial plane rotates towards the shear plane with increasing deformation.*	Figures 10 d,h, 11 a,e,f,j, 12 c, Tables 1f,4f
Acute angle between axial plane and foliation g) 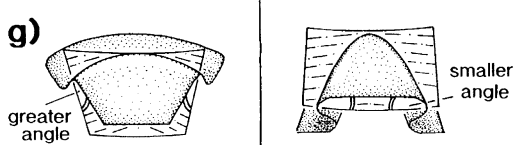	*With increasing shear strain, the acute dihedral angle, incorporating differences in both the strike and dip values of axial planes and the adjacent foliation, will reduce as the axial plane rotates towards the shear plane.*	**Greater angles -** Upper limbs / short hinge-lines **Smaller angles -** Lower limbs / long hinge-lines	**Cw angles -** S fold axial planes **A-Cw angles -** Z fold axial planes	*Thus, the **sense** of obliquity in the acute angle between the axial plane and the foliation is controlled by Z or S fold geometry, whilst the **amount** of obliquity will decrease as the axial plane rotates towards the shear plane with increasing deformation.*	Figures 9 i,j,k,l,m, 9 n,o,p, 10i,m, Tables 1g,4g

Similarly, long hinge-line segments typically trend closer to the transport direction and show greater (+ve) strain, compared with (− ve) short hinge line segments. Thus, vergence grids allow rapid assessment of 3-D vergence and strain patterns and are therefore of value in predicting and locating structural relationships that may be encountered in poorly exposed or less well constrained terranes.

5.2. Ranking grids

Reversals and reductions in both planar and linear obliquities across medial and axial surfaces effectively divide sheath folds into ranked quadrants as analysed on ranking grids. As noted in Section 4, strain variations across medial surfaces and large-scale axial surfaces result in differing degrees of fabric/fold deformation in each domain. Comparison of fold and fabric geometries, facing and amounts of rotation thus enables position on major structures to be accurately predicted (Fig. 12b). The structural parameters that display angular variations on passing from lower to higher strain may thus be measured and calculated from across axial surfaces and medial surfaces. The position on the major upper (− ve) or lower (+ve) fold limb is followed by location on either short (− ve) or long (+ve) hinge-line segments (Fig. 12b). Parameters may then be directly compared for each of the four quadrants (see Fig. 8 and Table 1), such that the highest strain relationship for any given parameter is ranked 1, whilst the lowest relative strain is designated 4 (Fig. 12b). Greatest fabric rotations (and hence deformation) are developed on the lower limbs forming the long hinge-line segments i.e. + ve and + ve end member of the ranking grid, whilst the lower strains are observed on the upper limbs forming short hinge-line segments (− ve and − ve scenario) (Fig. 12a and b). The greatest angular variation between north- and south-facing fold hinge trends and axial planar strikes is observed in − ve and − ve situations, whilst the least variation is in the highest strain scenarios (+ve and + ve). Thus, ranking grids provide a predictive statistical mechanism to determine overall relative strain patterns within and between structural domains as defined by medial and axial surfaces.

5.3. Rotation grids

Reversals in the sense of both axial planar and hinge rotations across medial and axial surfaces effectively divide sheath folds into antithetic and synthetic rotating quadrants as analysed on rotation grids. Within dome or basin settings, Z fold axial planar strike will display a clockwise rotation towards the foliation with increasing strain, whilst S fold axial planes display anticlockwise rotations (Fig. 12c) (see Section 3.5). The sense of fold hinge rotation is governed by position on major sheath folds, such that folds preserved in a clockwise sense to the extension lineation have undergone (incomplete) anticlockwise rotation, whilst anticlockwise hinges have suffered a clockwise rotation (Fig. 12c). The interplay of Z and S axial planes coupled with clockwise and anticlockwise rotating fold hinges therefore results in combinations of rotations which may be either in the same (synthetic) or opposing (antithetic) sense to one another in different structural quadrants of dome and basin geometries (Fig. 13). With increasing strain on the upper limbs of antiforms, fold hinges and axial surfaces on either side of the culmination surface consistently show antithetic senses of rotation, whilst synthetic rotations are observed on the lower fold limbs (Fig. 13a; Table 2). With increasing strain on the upper limbs of synforms, fold hinges and axial surfaces on either side of the depression surface consistently show synthetic senses of rotation, whilst antithetic rotations are observed on the lower fold limbs (Fig. 13b; Table 2). Thus, rotation grids enable distinct and diagnostic relationships between the variable senses of axial planar and fold hinge rotation to be clearly appreciated and analysed in 3-D.

6. Variation in structural relationships around major sheath folds

In addition to looking at the relative *sense* of obliquity between fabric elements, absolute amounts of deviation (irrespective of *sense*) between structural parameters may also be examined. Such an approach has the advantage of allowing total variations in fabric rotations to be directly compared both across axial surfaces and medial surfaces, which may otherwise display opposing obliquities.

6.1. Variation in fabrics across axial surfaces of major sheath folds

Attenuated (lower) limbs of sheath folds are marked by increasing rotation of planar and linear fabrics towards the shear plane and transport direction, respectively, and are thus not symmetrical about axial surfaces. Buckle folds that originally verged in the direction of shear may undergo

Fig. 8. Schematic sketches and summary text explaining the geometric consequences of fold and fabric rotations associated with increasing deformation. For each topological parameter ((a)–(g)), plan-view sketches illustrate the lower strain (− ve) and higher strain (+ve) relationship, whilst the adjacent notes summarise controls on the amounts and senses of fabric obliquity. Angular relationships between parameters may become greater or smaller with increasing deformation, whilst the sense of obliquity (viewed from above) is related to the reference datum as defined by the trend of the transport-parallel lineation (Ln) or strike of foliation (Sn). Refer to text and Table 1 for further discussion.

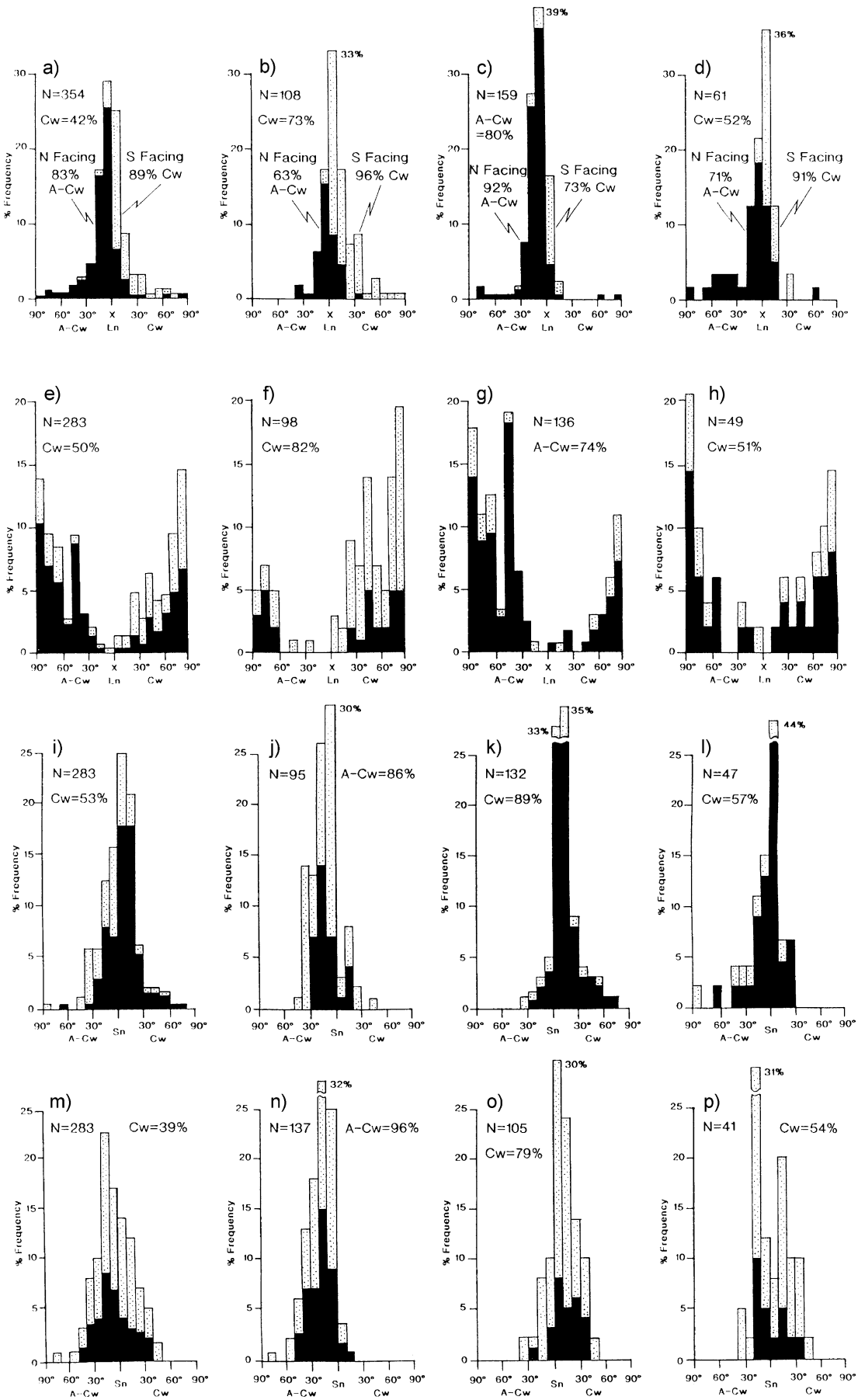
a)
N=354
Cw=42%
N Facing
83%
A-Cw
S Facing
89% Cw
b)
N=108
Cw=73%
N Facing
63%
A-Cw
S Facing
96% Cw
33%
c)
N=159
A-Cw
=80%
N Facing
92%
A-Cw
S Facing
73% Cw
39%
d)
N=61
Cw=52%
N Facing
71%
A-Cw
S Facing
91% Cw
36%
e)
N=283
Cw=50%
f)
N=98
Cw=82%
g)
N=136
A-Cw=74%
h)
N=49
Cw=51%
i)
N=283
Cw=53%
j)
N=95
A-Cw=86%
30%
k)
N=132
Cw=89%
35%
33%
l)
N=47
Cw=57%
44%
m)
N=283
Cw=39%
n)
N=137
A-Cw=96%
32%
o)
N=105
Cw=79%
30%
p)
N=41
Cw=54%
31%
% Frequency
A-Cw
Ln
Sn
Cw

severe modification during progressive shear resulting in highly attenuated lower fold limbs (Mies, 1993). On passing across the axial surface from an upper limb to a lower limb setting, both antiformal (Melness) and synformal (Sleiteil) dominated geometries display a systematic and predictable increase in strain reflected in the topological parameters (Fig. 13; Tables 3 and 4). Overall, a greater strain gradient appears across the axial surface in the antiformal (Melness) setting, possibly reflecting the geometry and orientation of the original buckle folds undergoing progressive shear. Thus, fabric patterns and relationships across both antiformal and synformal axial surfaces consistently indicate that upper fold limbs have undergone least rotation from original NNE-trending buckle fold hinges. As recognised by Fossen and Rykkelid (1990), such patterns, when combined with the direction of sheath closure, allow the relative shear sense to be determined.

6.2. Variation in fabrics across medial surfaces of major sheath folds

Attenuated (long) hinge-line segments of sheath folds are marked by increasing rotation of planar and linear fabrics towards the shear plane and transport direction, respectively, and are thus not symmetrical about medial surfaces. Sheath folds may display strain variations associated with asymmetric fold hinge-line vergence across culmination/depression surfaces (Alsop and Holdsworth, 1999). On passing across the medial surface from a short hinge-line to a long hinge-line setting, both culmination- (Melness) and depression- (Sleiteil) dominated settings display a systematic and predictable increase in strain reflected in the topological parameters (Tables 3 and 4). Note that such variations across medial surfaces are developed on both the upper and lower limbs of major sheath folds. This pattern is most obvious in Sleiteil and may reflect the original geometry and asymmetry of fold hinge-lines defining irregular synformal folding. The preservation in Melness of secondary medial surfaces trending marginally anticlockwise of the major culmination may reflect lower strains on the northern short hinge-line segment (Section 2). Thus, fabric patterns and relationships across medial surfaces associated with overall north-directed fold hinge-line vergence consistently indicate that short hinge-line segments have undergone least rotation from original NNE-trending buckle fold hinges.

6.3. Variation in elliptical eye-shaped patterns around major sheath folds

Classic elliptical sections through the nose of sheath folds may be asymmetric across both the axial surface and medial surface resulting in tear-drop eye folds. When sheath folds are viewed in the plane normal to both the axial surface and the medial surface (i.e. the Y–Z plane—see Fig. 1), pronounced hinge curvilinearity is marked by nested, eye-shaped rings representing cross-sections through the noses or caps of individual sheath folds. Where the extension lineation (X) acts as the bisector to the apical angle of the sheath fold (see Section 6.6 below), then such elliptical patterns are broadly symmetrical about the medial surface resulting in the classic eye-fold pattern frequently considered diagnostic of sheath folding. If the observed sections are oblique to the Y–Z plane then apparently asymmetric ellipses may be created by the variable oblique cut through each constantly orientated fold hinge-line segment.

Mies (1993) noted, however, that nested inner and outer elliptical rings through precise Y–Z sections of sheath folds were eccentric (i.e. without a common centre). The calculated centre of each successive outer elliptical ring was observed to transfer along the plane of bilateral symmetry (the medial surface) towards the thicker fold limb. This migration was considered a consequence of the relative thickening and/or thinning of individual fold limbs (measured parallel to the medial surface) across the axial surface. This interpretation of Mies (1993) can now be extended to variations in fold hinge thickness (measured parallel to the axial surface) across medial surfaces.

Where pronounced fold hinge-line vergence is associated with non-parallel fold hinges on either side of a medial surface, nested, asymmetric *tear-drop eye folds* are developed which are attenuated at one end and non-elliptical in section (Figs. 2, 14 and 15). Skjernaa (1989), describing detailed sheath fold geometries in the Scandinavian Caledonides, also notes that cross-sections through the noses of sheath folds may be attenuated at one end of the axial surface, whilst Lacassin and Mattauer (1985, their fig. 3) also clearly illustrate kilometre-scale Alpine examples of tear-drop eye folds. Within the nested eye pattern, the sense of migration of the centres of outer eyes compared with the inner rings

Fig. 9. Frequency distribution histograms of F2 fold hinges and axial planar strikes from Melness ((a)–(l)) and Sleiteil ((m)–(p)) orientated either clockwise (Cw) or anticlockwise (A-Cw) relative to the trend of the adjacent L2 extension lineation (X) ((a)–(h)) or foliation (Sn) strike ((i)–(p)). Data from north-facing domains is shown in solid whilst data from south-facing domains is stippled. Histograms show the trend (relative to X) of (a) all Melness F2 fold hinges, subdivided into (b) F2 Z fold hinges, (c) F2 S fold hinges, and (d) F2 M fold hinges. Histograms show the strike (relative to X) of (e) all Melness F2 axial planes, subdivided into (f) F2 Z axial planes, (g) F2 S axial planes, and (h) F2 M axial planes. Histograms show the acute angle and trend (relative to foliation (Sn) strike) of (i) all Melness F2 axial planes, subdivided into (j) F2 Z axial planes, (k) F2 S axial planes, and (l) F2 M axial planes. Histograms show the acute angle and trend (relative to foliation (Sn) strike) of (m) all Sleiteil F2 axial planes, subdivided into (n) F2 Z axial planes, (o) F2 S axial planes, and (p) F2 M axial planes. Overall in Melness and Sleiteil, S fold axial planar strike is 85% clockwise (Cw) of the foliation (Sn) trend, while Z fold axial planes are 92% anticlockwise of Sn. See text for further discussion.

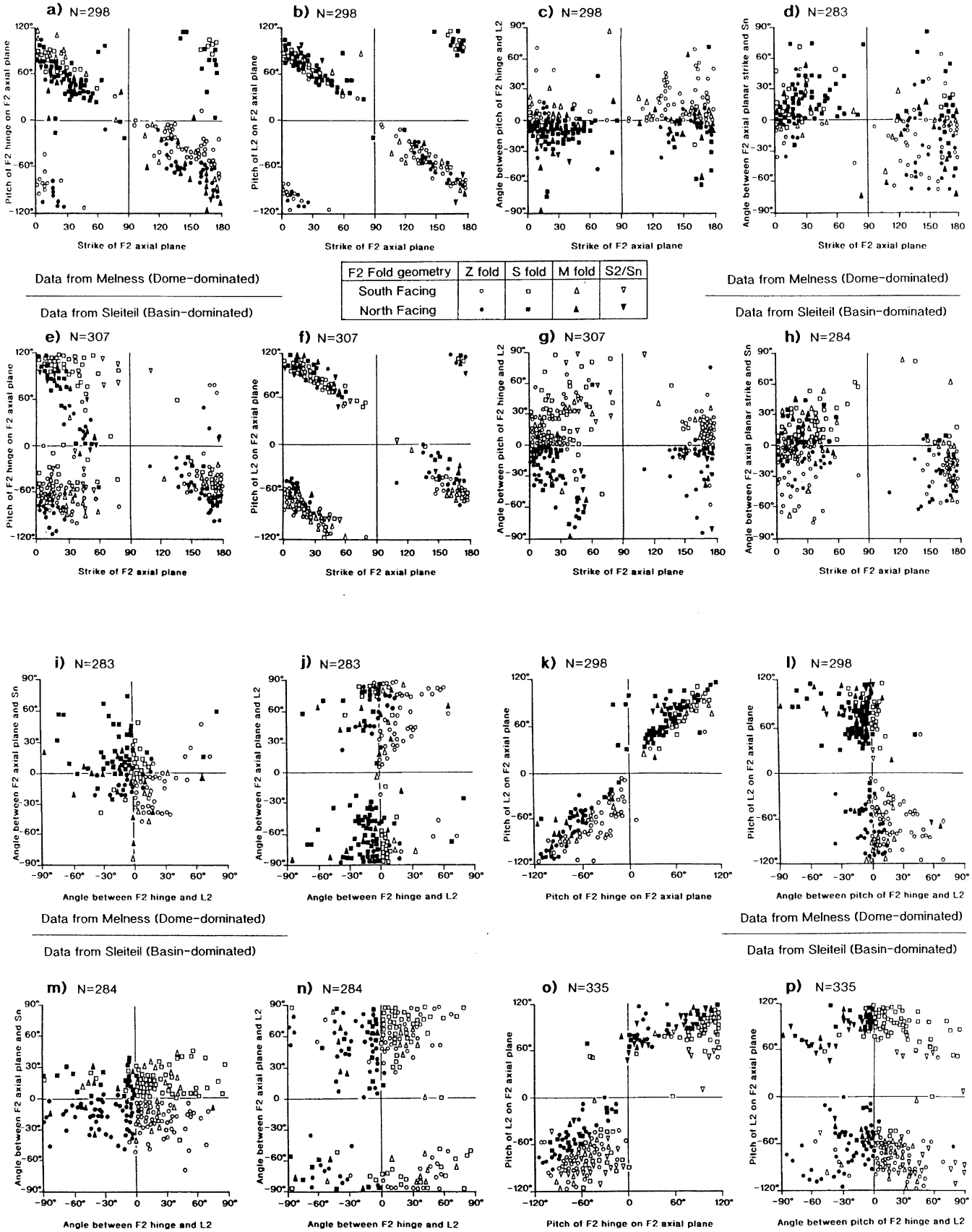
a) N=298
b) N=298
c) N=298
d) N=283
Pitch of F2 hinge on F2 axial plane
Pitch of L2 on F2 axial plane
Angle between pitch of F2 hinge and L2
Angle between F2 axial planar strike and Sn
Strike of F2 axial plane
Data from Melness (Dome-dominated)
Data from Sleiteil (Basin-dominated)
F2 Fold geometry
Z fold
S fold
M fold
S2/Sn
South Facing
North Facing
e) N=307
f) N=307
g) N=307
h) N=284
i) N=283
j) N=283
k) N=298
l) N=298
Angle between F2 axial plane and Sn
Angle between F2 axial plane and L2
Angle between F2 hinge and L2
Pitch of F2 hinge on F2 axial plane
Angle between pitch of F2 hinge and L2
m) N=284
n) N=284
o) N=335
p) N=335

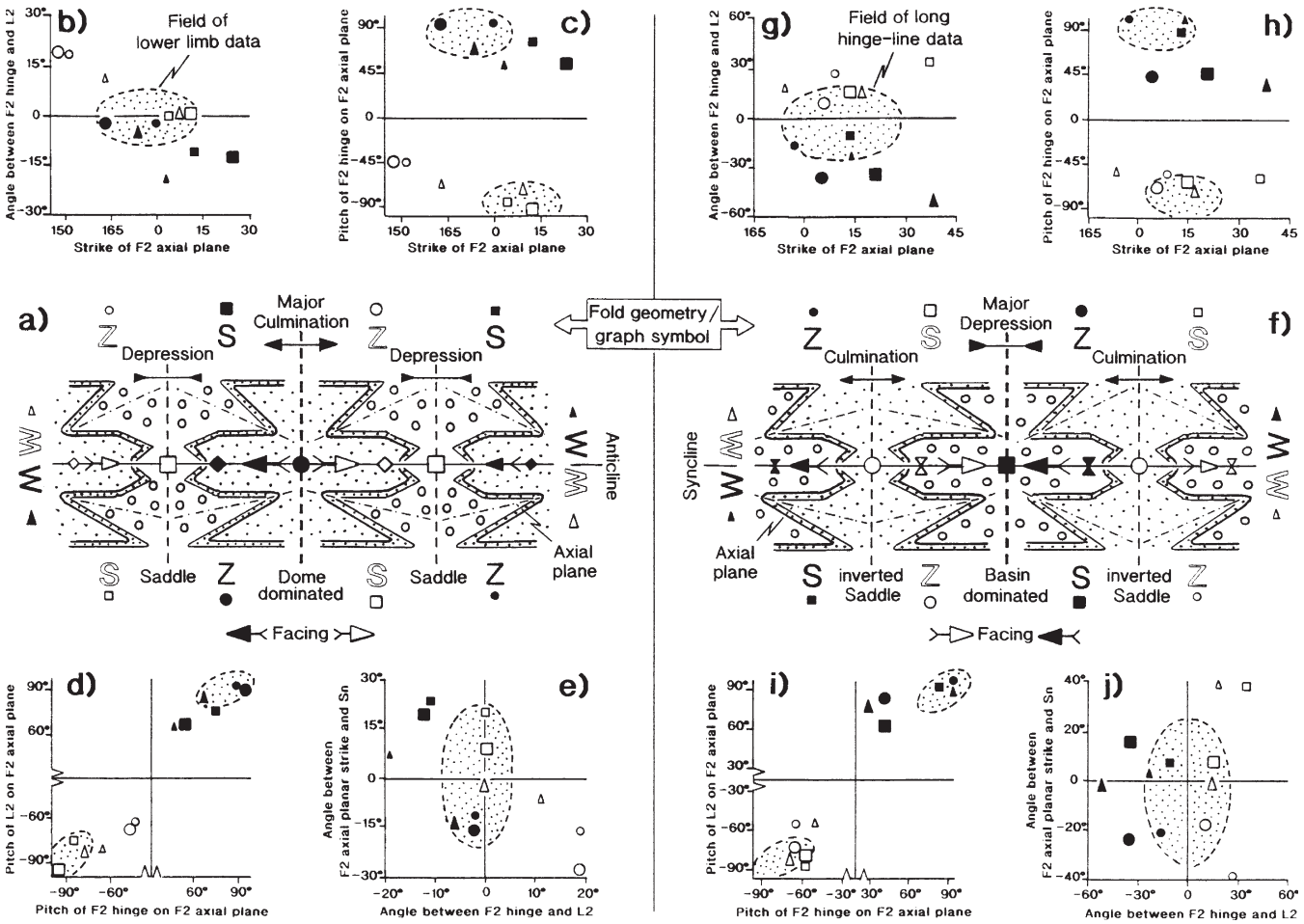

Fig. 11. Transport-normal sections and analyses of dome-dominated deformation patterns in Melness (a) and basin-dominated patterns in Sleiteil (f). In each case, north-facing folds are shown by the solid symbols whilst south-facing structures are given by the open symbols. Dominant fold geometries developed on long hinge-line segments are shown with larger symbols in each case and correspond to the orientation of the mean data sets shown on the summary fabric topology plots. Plots showing the mean strike of F2 axial planes are compared with ((b) and (g)) the mean angle between F2 hinges and L2 and ((c) and (h)) the pitch of the F2 hinge. (d) and (i) The pitch of mean F2 hinges on associated F2 axial planes compared with the pitch of L2 on F2 axial planes. (e) and (j) Angle between mean F2 hinges and L2 compared with the angle between F2 axial planar strike and Sn. Note that the mean data from the lower fold limbs and/or the long hinge-line segments is highlighted in stipple and consistently plots in higher strain relationships.

(or 'pupils') is along the axial surface and towards the major culmination surface in domal sheath folds (Fig. 15c), and towards the major depression surface in basinal sheaths (Fig. 15d). Thus within tear-drop eye folds which have undergone layer attenuation across both axial surfaces and medial surfaces, the centres of inner eyes are located off-centre compared with outer rings. The lack of a common centre coupled with a consistent sense of offset (within the Y–Z plane) provides a means of determining patterns of minor fold limb/fold hinge-line vergence and the location of major axial and/or medial surfaces.

Fig. 10. Fabric topology plots of F2 fold and fabric data from a high strain dome-dominated setting (Melness, upper row) and a lower strain basin-dominated scenario (Sleiteil, lower row). South-facing data is shown by open symbols whilst north-facing data is shown by closed (solid) symbols. In each case, structures associated with Z (circles), S (squares), or M (triangles) folds are shown with +ve clockwise (Cw) or −ve anticlockwise (A-Cw) relationships. Whilst strike values are given between 0 and 180°, values of pitch are taken beyond 90° (i.e. down-dip) up to 120°, in order to show the continuation of geometric trends across the dip-direction. Plots show how the strike of the F2 axial plane controls the relative pitch of the F2 fold hinges on the associated axial planes in (a) Melness and (e) Sleiteil (below). Plots show how the strike of the F2 axial plane controls the relative pitch of the L2 extension lineation on the associated axial planes in (b) Melness and (f) Sleiteil (below). Plots show how the strike of the F2 axial plane varies in relation to the acute angle between the pitch of the F2 hinge and L2 as measured on the axial plane in (c) Melness and (g) Sleiteil. Plots show how the strike of F2 axial planes varies with the angle between the strike of the axial plane and the adjacent foliation (Sn) surface in (d) Melness and (h) Sleiteil (below). Plots show how the angle between F2 fold hinges and L2 varies in relation to the acute angle between the axial plane and Sn in (i) Melness and (m) Sleiteil. Plots show how the angle between F2 hinges and L2 varies with the angle between F2 axial planar strike and L2 in (j) Melness and (n) Sleiteil. Plots show how the pitch of F2 hinges on the associated axial plane varies in relation to the pitch of the L2 in (k) Melness and (o) Sleiteil (below). Plots show how the acute angle between the pitch of F2 hinges and L2 varies with the pitch of L2 on F2 axial planes in (l) Melness and (p) Sleiteil (below).

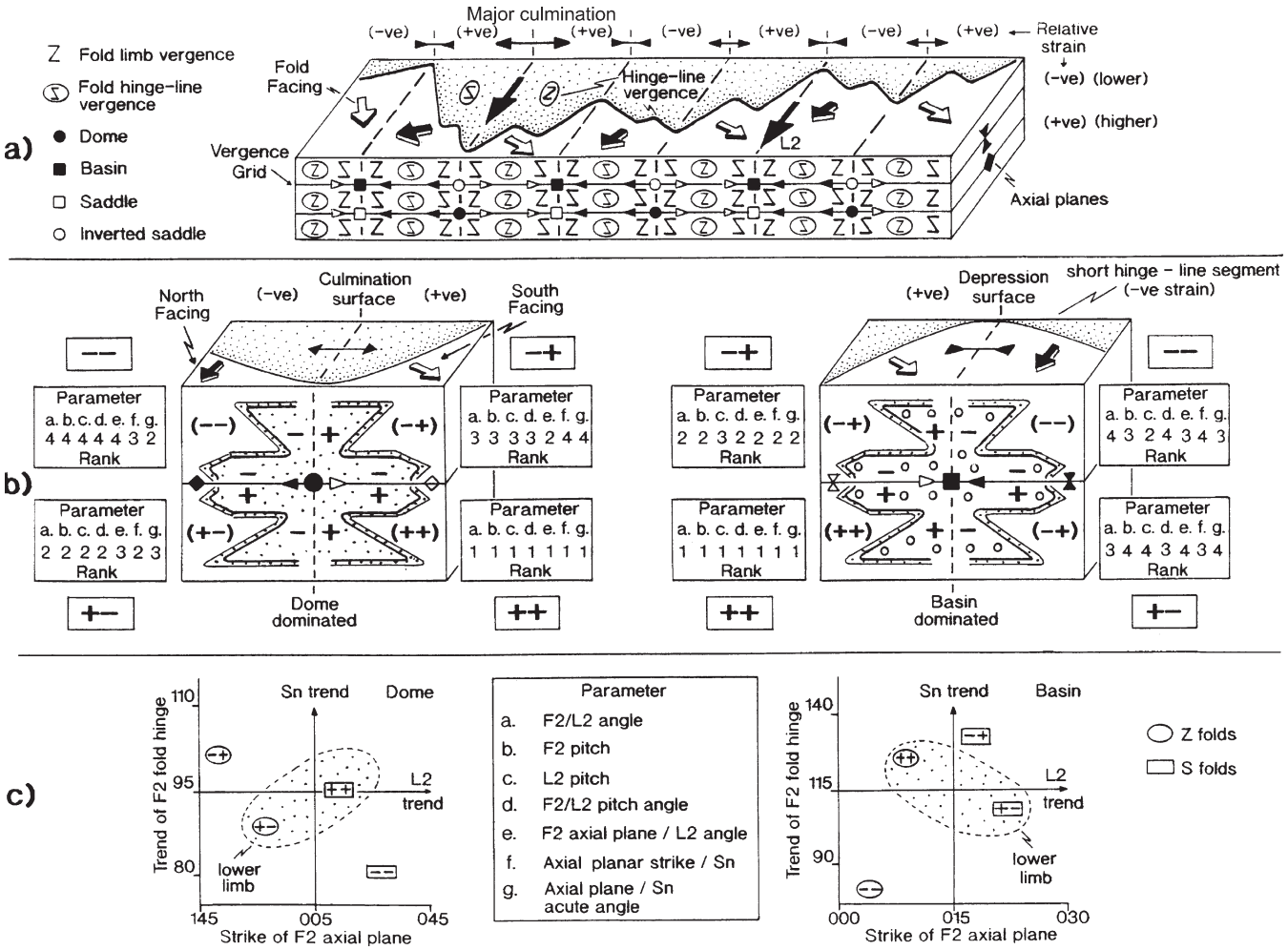

Fig. 12. (a) Schematic 3-D *vergence grid* illustrating the interplay between fold hinge-line vergence and fold limb vergence. The relative location of culmination/depression surfaces and antiformal/synformal axial planes results in the range of dome and basin scenarios depicted. The upper limbs of folds display lower strain (− ve) than the adjacent lower limb (+ve). Note that the long hinge-line segments of curvilinear fold hinge lines display greater (+ve) strain than adjacent short hinge line segments (− ve). The major culmination labelled on the diagram is associated with long hinge-line segments (and therefore higher (+ve) strain) on both margins. Adjacent (secondary) culmination and depression surfaces separate long and short hinge line segments associated with greater and lower strain on each margin. (b) and (c) Analysis of dome-dominated and basin-dominated end-member scenarios from Melness and Sleiteil, respectively. In each location, the upper limb consistently represents lower (− ve) strain, whilst the north-facing fold hinge-line is the short segment and also represents (− ve) strain. Relative strain for fold limbs is consistently followed by relative strain for short or long hinge-lines resulting in the (− −), (− +), (+ −) and (++) scenarios. For each case, strain parameters (a) − (g) have been ranked from 1 (greatest strain) to 4 (lowest strain). Fabric parameters consistently indicate greater strain in (++) scenarios and lower strain in (− −) situations. (c) Plots showing the orientation of Z and S fold hinges and axial planes relative to mean L2 trends and strike of F2 axial planes. Note how Z and S fold axial planes are consistently anticlockwise and clockwise of the mean Sn trend, whilst north- and south-facing fold hinges are anticlockwise and clockwise of L2 (respectively). Data from the higher strain lower fold limb are highlighted in stipple in each case.

6.4. Variation in bedding/cleavage intersections around major sheath folds

Bedding-cleavage intersection lineations transect minor folds trending clockwise and anticlockwise of transport with consistent relative obliquities, thus confirming the sense of hinge rotation and polarity of fold facing in sheath folds. The angle of transection is measured between the trend of the fold hinge (datum) and the associated bedding/cleavage intersection lineation. Gentle transection of sheath folds by the S2 cleavage is a consequence of the major fold limbs and axial surfaces of minor sheath folds being mildly curviplanar about the transport (X) direction and preserving incomplete rotation into the foliation (X–Y) plane. As noted previously (Section 3.4; Figs. 6b, 7a–c and 11a and f), the limbs of major sheath folds remain parallel or ‘bow-out’ around dome and basin configurations, whilst S2 parallels the axial surfaces of minor folds which ‘converge’ towards domes and basins (Fig. 13a and b). Axial planar S2 therefore displays an opposing obliquity to the ‘bowed’ regional foliation about the medial surface, thereby resulting in a small but consistent sense of transection on either margin of the sheath fold.

Table 1
Summary table highlighting the various causes and controls between the seven topological parameters and their relationships to increasing deformation. When viewed from above, fold hinges and axial planes may rotate in a clockwise (Cw) or anticlockwise (A-Cw) sense towards the reference datum defined by the trend of the lineation (Ln) and strike of foliation (Sn). Refer to Fig. 8 and text for further details

Topological Parameter	Observation	Cause	Control on Obliquity	Sense of Rotations	Topological Relationships	Lower strain Patterns	Higher strain Patterns	Table / Figure Reference
a) *Angle between trend of fold hinge and Ln*	**a)** reduces with greater deformation	Rotation of fold hinge towards X	Sense of hinge rotation	S facing hinges rotate A-Cw N facing hinges rotate Cw	S facing hinges trend Cw of Ln N facing hinges trend A-Cw of Ln	Broad arc of hinge trends (<90°) to Ln	Cluster of hinge trends sub-parallel (<20°) to Ln	Table 4a Figures 8a, 9a,b,c,d, 10i,j,m,n 11a,b, 12c
b) *Angle of pitch of fold hinge on axial plane*	**b)** increases with greater deformation	Rotation of fold hinge and axial plane towards X and X-Y respectively	Sense of hinge and axial plane rotation	S facing hinges & S axial planes rotate A-Cw N facing hinges & Z axial planes rotate Cw	S axial plane = Cw hinge pitch Z axial plane = A-Cw hinge pitch	Low values (<65°) of hinge pitch	High values (<90°) of hinge pitch	Table 4b Figures 8b, 10a,e, 11a,c,f,h,
c) *Angle of Ln pitch on axial plane*	**c)** increases with greater deformation	Rotation of axial plane towards X-Y plane	Sense of axial plane rotation	S axial planes rotate A-Cw Z axial planes rotate Cw	S axial plane = Cw Ln pitch Z axial plane = A-Cw Ln pitch	Low values (<75°) of Ln pitch	High values (<90°) of Ln pitch	Table 4c Figures 8c, 10b,f, 11a,d,f,i,
d) *Angle between pitch of fold hinge and Ln*	**d)** reduces with greater deformation	Rotation of fold hinge and axial plane towards X and X-Y respectively	Sense of hinge and axial plane rotation	S facing hinges & S axial planes rotate A-Cw N facing hinges & Z axial planes rotate Cw	S facing hinges pitch Cw of Ln N facing hinges pitch A-Cw of Ln	Large differences (<30°) in fold hinge and Ln pitch values	Small differences (<10°) in fold hinge and Ln pitch values	Table 4d Figures 8d, 10c,g,k,l,o,p 11a,d,f,i,
e) *Angle between strike of axial plane and Ln trend*	**e)** increases with greater deformation	Rotation of axial plane towards X-Y plane	Sense of axial plane rotation	S axial planes rotate A-Cw Z axial planes rotate Cw	S axial plane strikes A-Cw of Ln Z axial plane strikes Cw of Ln	Axial planes strike oblique (<60°) to Ln trend	Axial planes strike sub-normal (<80°) to Ln trend	Table 4e Figures 8e, 9e,f,g,h, 10j,n 12c
f) *Angle between strikes of axial plane and Sn*	**f)** reduces with greater deformation	Rotation of axial plane towards X-Y plane	Sense of axial plane rotation	S axial planes rotate A-Cw Z axial planes rotate Cw	S axial plane strikes Cw of Sn Z axial plane strikes A-Cw of Sn	Axial planes strike oblique (<30°) to Sn trend	Axial planes strike sub-parallel (<10°) to Sn trend	Table 4f Figures 8f, 10d,h, 11a,e,f,j, 12c,
g) *Acute angle between axial plane and Sn*	**g)** reduces with greater deformation	Rotation of axial plane towards X-Y plane	Sense of axial plane rotation	S axial planes rotate A-Cw Z axial planes rotate Cw	S axial plane = Cw of Sn Z axial plane = A-Cw of Sn	Axial planes oblique (<20°) to Sn	Axial planes sub-parallel (<15°) to Sn	Table 4g Figures 8g, 9i,j,k,l,m, 9n,o,p, 10i,m

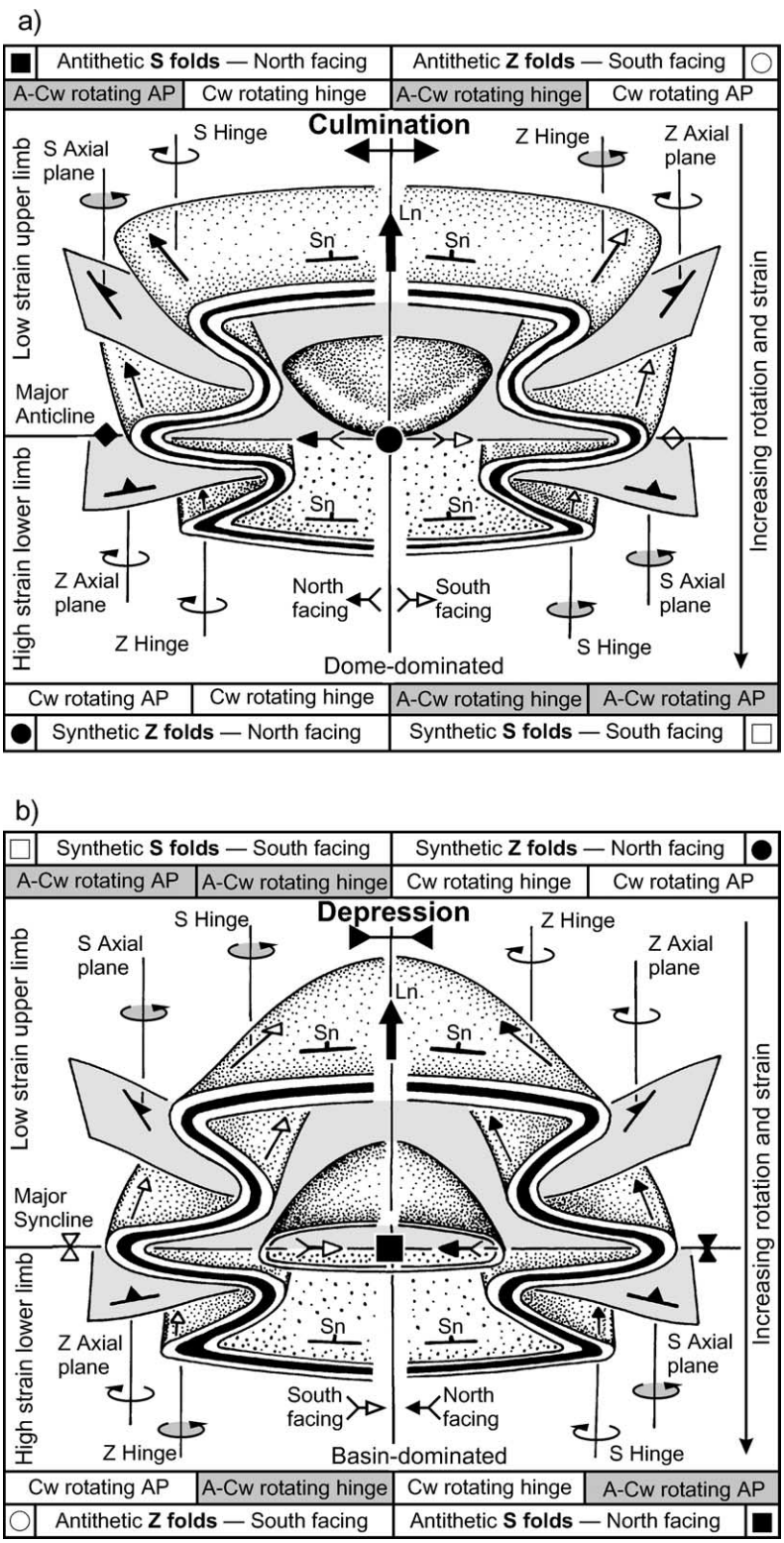

Fig. 13. Schematic summary figure of fabric rotations associated with (a) a dome (antiform on culmination) geometry and (b) a basin (synform on depression) configuration. Strain, and hence fold hinge and axial planar rotation, increases from the upper to lower limbs of sheath folds. The rotation of an axial plane is measured through variations in strike and is governed by the Z or S fold geometry, whilst the sense of rotation of fold hinges is dependent on the fold facing direction and position relative to medial surfaces. In each case, anticlockwise rotations are highlighted in grey tone. Fold hinges may thus rotate with increasing strain in either the same (synthetic) or opposing (antithetic) sense to the associated axial plane depending on structural setting.

Table 2
Summary table of fabric *rotation grid* associated with a dome (antiform on culmination) geometry (top) and basin (synform on depression) configuration (bottom). In each case, incomplete clockwise rotation (relative to the Ln trend) will result in the preservation of anticlockwise obliquities and visa versa. The rotation of an axial plane is measured through variations in strike and is governed by the fold geometry, whilst the sense of rotation of fold hinges is dependent on the fold facing direction and position relative to medial surfaces. Fold hinges may thus rotate with increasing strain in either the same (synthetic) or opposing (antithetic) sense to the associated axial plane depending on structural setting

Dome Geometry	**Culmination surface**	
	Anticlockwise hinge obliquity	Clockwise hinge obliquity
Upper limb Antithetic rotation	**S Folds** Clockwise rotating hinge Anticlockwise rotating axial plane	**Z Folds** Anticlockwise rotating hinge Clockwise rotating axial plane
Antiformal axial plane		
Lower limb Synthetic rotation	**Z Folds** Clockwise rotating hinge Clockwise rotating axial plane	**S Folds** Anticlockwise rotating hinge Anticlockwise rotating axial plane

Basin Geometry	**Depression surface**	
	Clockwise hinge obliquity	Anticlockwise hinge obliquity
Upper limb Synthetic rotation	**S Folds** Anticlockwise rotating hinge Anticlockwise rotating axial plane	**Z Folds** Clockwise rotating hinge Clockwise rotating axial plane
Synformal axial plane		
Lower limb Antithetic rotation	**Z Folds** Anticlockwise rotating hinge Clockwise rotating axial plane	**S Folds** Clockwise rotating hinge Anticlockwise rotating axial plane

The lineation generated by the intersection of the axial planar S2 cleavage with the foliation (Sn) displays a greater deviation from L2 than associated minor fold hinges (Figs. 4 and 7f). The intersection lineation within north-facing domains is developed anticlockwise of the mean north-facing folds, and within south-facing domains is clockwise of south-facing folds. The bedding cleavage intersection lineation also shows the greatest angular variation between long and short hinge-line segments. This is especially pronounced on the upper limbs of sheath folds in short hinge-line segments, i.e. in the lowest strain (−ve and −ve) scenarios (see Fig. 12b). Greater angles of S2 transection are typically developed in these lower strain settings as axial surfaces of minor folds and foliation preserve the greatest obliquity and curviplanarity. In addition, bedding/S2 intersections on long hinge line segments display smaller angles between S2 intersection/L2 trends, smaller angles between S2 intersection/L2 pitches, and larger angles of S2 intersection pitch all of which support greater deformation on the long hinge-line segments.

In summary, the bedding-cleavage intersection lineation demonstrates consistent senses of transection across fold hinges and therefore indicates (and predicts) the sense of fold rotation within that domain. In the absence of younging criteria, the sense of cleavage transection may thus be analysed in order to confidently determine the direction of fold rotation in much the same way as fold facing is typically employed.

6.5. Variation in neutral verging folds around major sheath folds

Neutral verging M folds developed along the axial surface of sheath folds accurately portray fabric rotations across medial surfaces, thereby defining patterns of asymmetric fold hinge-line vergence. In higher strain scenarios, the overturned limbs of folds are rotated sub-parallel to the extension lineation and angular obliquities may be increasingly difficult to measure. In addition, S and Z folds 'switch' positions from upper to lower limbs across axial surfaces and also on passing across medial surfaces, thus complicating comparisons of rotation (e.g. Fig. 13). However, neutral-verging M folds maintain a 'fixed' relative position along axial surfaces and are clearly better suited to direct comparisons of deformation and rotation across the medial surfaces.

On passing across the medial surface from short hinge-line to a long hinge-line setting, neutral verging folds in both culmination- (Melness) and depression- (Sleiteil) dominated settings display systematic and predictable variation in the structural parameters (Tables 3 and 4). Short hinge-line segments undergo less rotation and deformation than long hinge-line sections (Table 4). Thus, analysis of neutral verging M fold geometries provides valuable information on the geometry of curvilinear hinge-lines associated with asymmetric fold hinge-line vergence, and thereby provides a means of consistently and accurately determining deformation about medial surfaces.

Table 3
Summary table of angular obliquities associated with topological parameters in the Melness (top) and Sleiteil (bottom) areas. Each table summarises mean data across the axial surface of major folds (upper and lower limbs), together with mean data from short and long hinge-line segments across the major culmination (Melness) or depression (Sleiteil) surfaces. In each case, data refers to the angular difference (rather than *sense* of obliquity) and indicates that lower fold limbs and long hinge-line segments have undergone greater deformation. Structural parameters: (a) angle between trend of fold hinge and lineation, (b) angle of fold hinge pitch on axial plane, (c) angle of lineation pitch on axial plane, (d) angle between pitch of fold hinge and lineation, (e) angle between axial planar strike and lineation trend, (f) angle between axial planar strike and trend of foliation, and (g) acute angle between axial plane and long-limb foliation

Melness	**Antiformal Axial Surface**			**Culmination Surface**		
Topological Parameter	Upper Limb (-ve)	Lower Limb (+ve)	**Angular Difference**	Short Hinge (-ve)	Long Hinge (+ve)	**Angular Difference**
a)	15°	1°	**-14°**	9°	8°	**-1°**
b)	56°	84°	**+28°**	71°	79°	**+8°**
c)	71°	83°	**+12°**	76°	85°	**+9°**
d)	13°	2°	**-11°**	13°	7°	**-6°**
e)	65°	74°	**+9°**	64°	75°	**+11°**
f)	22°	14°	**-8°**	18°	18°	**0°**
g)	17°	14°	**-3°**	16°	14°	**-2°**

Sleiteil	**Synformal Axial Surface**			**Depression Surface**		
Topological Parameter	Upper Limb (-ve)	Lower Limb (+ve)	**Angular Difference**	Short Hinge (-ve)	Long Hinge (+ve)	**Angular Difference**
a)	26°	21°	**-5°**	34°	14°	**-20°**
b)	62°	65°	**+3°**	52°	75°	**+23°**
c)	83°	76°	**-6°**	80°	90°	**+10°**
d)	23°	15°	**-8°**	31°	13°	**-18°**
e)	69°	73°	**+4°**	62°	80°	**+18°**
f)	23°	21°	**-2°**	30°	14°	**-16°**
g)	18°	19°	**+1°**	22°	16°	**-6°**

6.6. Variation in apical angles around major sheath folds

Apical angles of sheath folds are found to systematically reduce from upper to lower limbs across the axial surface, and also from short hinge-line to long hinge-line segments around medial surfaces of sheath folds. The apical angle of a sheath fold is the acute angle between sections of a curvilinear hinge-line which have undergone an opposing sense of rotation, and hence display a reversal in the polarity of facing on the axial (X–Y) surface. Apical angles systematically reduce across the axial surfaces of major sheath folds (in both Melness and Sleiteil), with the upper limbs characterised by the largest apical angles which undergo a progressive reduction to the lower fold limb

Table 4
Summary table highlighting variations in topological parameters between upper and lower limbs of sheath folds and short and long hinge-line segments. The table also summarises variations in neutral verging M fold geometries and the apical angles of sheath folds. Refer to text for further discussion

Topological Parameter	**Upper limb of sheath fold**	**Lower limb of sheath fold**	**Short hinge-line segment**	**Long hinge-line segment**	**M folds – short hinge-lines**	**M folds – long hinge-lines**
a)	Greater angle	Smaller angle	Greater angle	Smaller angle	Greater angle	Smaller angle
b)	Smaller angle	Greater angle	Smaller angle	Greater angle	Smaller angle	Greater angle
c)	Smaller angle	Greater angle	Smaller angle	Greater angle	Smaller angle	Greater angle
d)	Greater angle	Smaller angle	Greater angle	Smaller angle	Greater angle	Smaller angle
e)	Smaller angle	Greater angle	Smaller angle	Greater angle	Smaller angle	Greater angle
f)	Greater angle	Smaller angle	Greater angle	Smaller angle	Greater angle	Smaller angle
g)	Greater angle	Smaller angle	Greater angle	Smaller angle	Greater angle	Smaller angle
Apical angle	Greater angle	Smaller angle	Greater angle	Smaller angle	Greater angle	Smaller angle

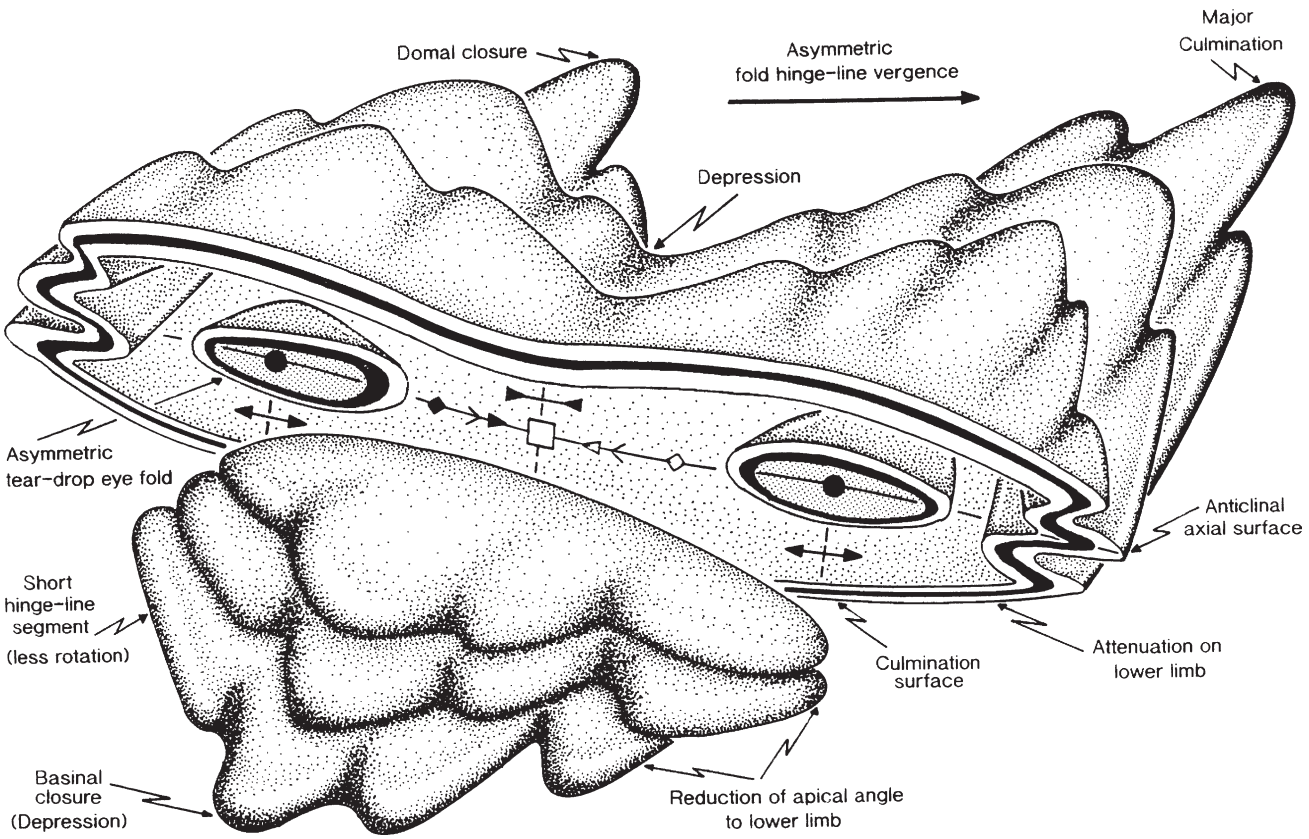

Fig. 14. Schematic 3-D cartoon illustrating asymmetric fold hinge-line vergence and increasing deformation towards a major culmination on the right of the sketch. Increasing deformation also results in pronounced attenuation on the lower fold limb and reduction in the apical angle of the sheath fold from tongue folds on the upper limb to tubular folds on the lower limb. Refer to text for further details and Fig. 12a for structural symbols.

where the apical angle is symmetrically bisected by the medial surface (Table 5) (Figs. 2 and 14). Apical angles on the lower limb of the dome-dominated Melness setting are consistent with curvilinear hinge-lines defining sub-isoclinal (2°) hairpin (or tubular) geometries, whilst the upper limb of the short hinge-line segment in Sleiteil records an apical angle of 72° reflecting a tongue fold morphology. Thus, extreme variations in the curvilinearity and apical angles of fold hinge-lines are observed within different structural positions of major individual sheaths.

Apical angles also systematically vary on either margin of major medial surfaces (Table 5). The major culmination surface in Melness displays a smaller mean apical angle as it juxtaposes two (higher strain) long hinge-line segments (Table 5). L2 acts as the bisector of the apical angle associated with the major culmination, with long hinge-line segments displaying more acute apical angles than the adjacent short hinge-lines although an overall symmetry is maintained. Contrary to the broadly symmetrical patterns developed across the culmination at Melness, south-facing folds on either margin of the depression at Sleiteil have undergone consistently greater rotations thereby resulting in L2 and the depression surface asymmetrically bisecting the apical angle (Table 5). Thus, asymmetric fold hinge-line vergence associated with variable apical angles is clearly developed across the major depression surface in Sleiteil (Table 5). In sheath folds marked by such pronounced fold hinge-line vergence, the long hinge-line segments are preferentially rotated into sub-parallelism with the extension lineation that thus asymmetrically bisects the apical angle. Apical angles may therefore be symmetrically or asymmetrically bisected by the extension lineation depending on the degree of fold hinge-line vergence about major medial surfaces (Fig. 15).

Thus, the *sense* in which the apical angle is asymmetrically bisected by the transport-parallel medial surface is dependent on the sense of long hinge-line rotation, whilst the *amount* of apical angle will decrease (with increasing strain) across axial surfaces from the upper to lower limbs and also across medial surfaces from short hinge-line to long hinge-line segments of sheath folds.

7. Discussion

The intensive study of minor sheath folds has enabled a detailed analysis of the factors that influence the geometry and evolution of individual folds (e g. Skjernaa, 1989; Crispini and Capponi, 1997). Large (kilometre-scale) sheath folds have been investigated (e.g. Vollmer, 1988; Goscombe, 1991; Beunk and Page, 2001; Hanmer and Greene, 2002), whilst general structural patterns within

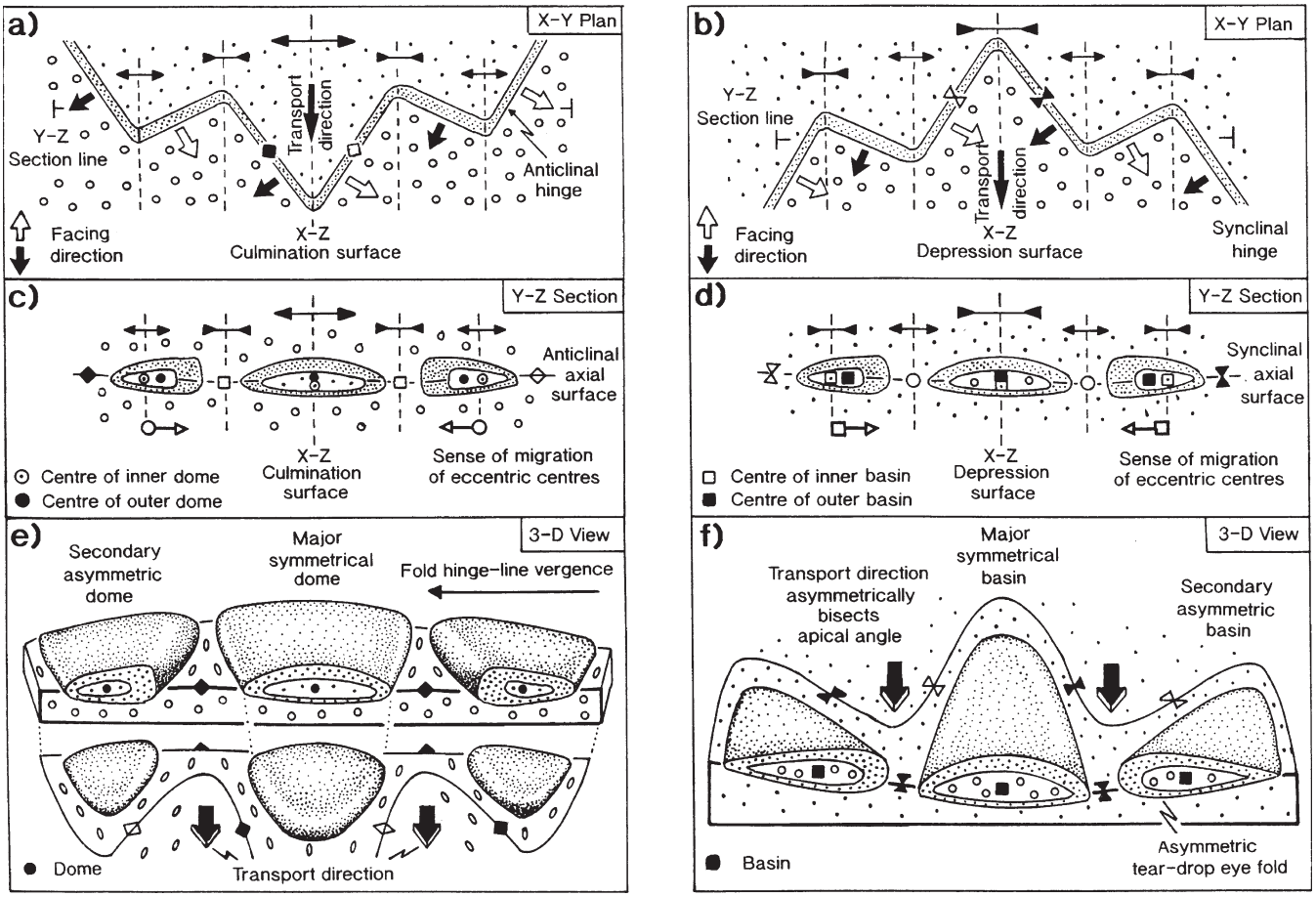

Fig. 15. Plan views (X–Y sections) across asymmetric fold hinge-line vergence forming a major culmination (a) and depression (b). Closely stippled unit represents the axial surface thickness of a bed bounded on each side by adjacent hinge-lines. Y–Z sections through domes (c) and basins (d) illustrate the relative migration of the eccentric centres of the tear-drop eye folds towards the major culmination and depression surfaces, respectively. In each case, the centre of the outer ring has migrated relative to the inner ring, and towards the associated major culmination (c) and depression surface (d). Neutral hinge-line vergence in both domes and basins is marked by migration of the eccentric centres towards the thicker fold limb. 3-D cartoons illustrate the overall asymmetry of domes (e) and basins (f) generated by variable amounts of rotation associated with fold hinge-line vergence. Refer to text for further details.

major sheath folding have also been documented (e.g. Alsop and Holdsworth, 1999). However, despite the general interest and possible economic benefits of understanding sheath geometries associated with mineralisation (e.g. Park, 1988; D'el-Roy Silva and Barros Neto, 2002), the precise mechanisms and kinematics of sheath folds, together with the geometry and orientations of folds which act as precursors to sheaths remain debateable and poorly understood.

7.1. Mechanisms of sheath folding

Whilst it is not the primary intention of this paper to discuss in detail the various mechanisms for the formation of sheath folds, it is noteworthy that traditionally, they are considered to form by the rotation of fold hinges which initiate at a high angle to shear during progressive non-coaxial deformation (e.g. Cobbold and Quinquis, 1980). However, generation of sheath folds by a simple shear mechanism necessitates large shear strains (γ in excess of 10; Hudleston, 1986), with apical angles of $<20^{\circ}$ producing X–Y aspect ratios of 35:1 (Skjernaa, 1989). Possible alternative mechanisms for generating sheath folds have therefore been considered and include constrictional deformation (e.g. Ez, 2000), constrictional non-coaxial deformation (e.g. Fletcher and Bartley, 1994; Fletcher et al., 1995), and general shear associated with shortening across the shear zone (e.g. Ghosh et al., 1999) (see Jiang and Williams, 1999). In addition, fold hinges that trend parallel to the direction of shear and initiate oblique to the shear plane, may subsequently undergo extension and have also been suggested as precursors to sheath folds (Skjernaa, 1989; Fletcher and Bartley, 1994; Boettcher and Mosher, 1998).

The preservation within this case study of variable angles of obliquity between fold hinges and the extension lineation, marked by stereographic distribution arcs of up to 180° in lower strain settings, indicates that the sub-parallelism and clustering of fold hinges and lineations observed on the higher strain lower limbs has been achieved through significant rotation of originally transport-normal hinges towards the shear direction. In addition, sheath folds display

Table 5
Summary table of hinge/lineation obliquities and associated apical angles of sheath folds from the dome-dominated Melness setting (top) and the basin-dominated Sleiteil setting (bottom). Each table summarises mean fold/lineation data and apical angle data (bold) across the axial surface of major folds (upper and lower limbs), together with mean data from hinge zones. Data is also summarised from north and south of the major culmination (Melness) or depression (Sleiteil) surfaces. In each case, fold hinges trending clockwise (Cw) or anticlockwise (A-Cw) of the extension lineation (datum) are described as + ve and − ve respectively. Apical angle data refers to the angular difference between the north- and south-facing domains and indicates that lower fold limbs and long hinge-line segments have undergone greater deformation

F2/L2 Angle	Northern Depression			Major Culmination	Southern Depression			Melness (dome)
Structural Position	South Facing (Cw)	Apical Angle	North Facing (A-cw)	Apical Angle	South Facing (Cw)	Apical Angle	North Facing (A-cw)	Mean Apical Angle
Upper Limb	+19°	**31°**	-12°	**31°**	+19°	**30°**	-11°	**31°**
Hinge	+11°	**17°**	-6°	**5°**	-1°	**19°**	-20°	**14°**
Lower Limb	-1°	**2°**	-3°	**3°**	0°	**2°**	-2°	**2°**
Mean Angle	+10°	**17°**	-7°	**13°**	+6°	**17°**	-11°	**16°**

F2/L2 Angle	Northern Culmination			Major Depression	Southern Culmination			Sleiteil (basin)
Structural Position	North Facing (A-cw)	Apical Angle	South Facing (Cw)	Apical Angle	North Facing (A-cw)	Apical Angle	South Facing (Cw)	Mean Apical Angle
Upper Limb	-16°	**32°**	+16°	**53°**	-37°	**72°**	+35°	**52°**
Hinge	-23°	**38°**	+15°	**67°**	-52°	**70°**	+18°	**58°**
Lower Limb	-11°	**22°**	+11°	**46°**	-35°	**62°**	+27°	**43°**
Mean Angle	-17°	**31°**	+14°	**55°**	-41°	**68°**	+27°	**51°**

larger apical angles on upper limbs which may be asymmetrically bisected by the medial surface and extension lineation, whilst the lower limbs define more acute apical angles which are symmetrically disposed about the extension lineation, thus confirming that pronounced fold rotations have generated the observed sheath morphology. The systematic reduction in the apical angle from the upper to lower limbs is interpreted to be a consequence of increasing fold rotation associated with significant strain gradients and non-coaxial deformation (Figs. 2 and 14). Marked variability in deformation across the axial surface of sheath folds (thus preserving sedimentary details for facing analysis) also suggests that simple models of intense non-coaxial shear *uniformly* affecting pre-existing fold geometries may overestimate bulk displacements and shear strain.

The amplification and growth of major nappes, which may display sheath geometries is poorly understood and relates to two principal models (e.g. Platt, 1982). The first model relates to rolling fold hinges in which the major hinge migrates with respect to the limbs, resulting in material and minor structures progressively passing around the hinge from the upper to lower limb in a 'conveyor belt' fashion. Minor folds would thus pass around the major hinge, resulting in an apparent reversal in asymmetry across the axial surface (S to Z, etc.), whilst the facing polarity remains the same. Such a process would also result in the sense of hinge/lineation obliquity reversing from upper to lower limbs when viewed from above. However, this study has shown that the sense of hinge/lineation obliquity consistently corresponds to the direction of fold facing on both the upper and lower limbs of sheath folds, thus making the rolling hinge model inapplicable. The alternative model assumes that the fold hinge remains fixed with respect to the limbs and that increasing fold amplitude is achieved via attenuation of the lower limb during intense non-coaxial deformation. The patterns of increasing deformation on overturned limbs accord well with this model, which is therefore preferred. It has thus been possible to unequivocally demonstrate using FTPs that sheath geometries within this study are the product of variable fold hinge rotation during heterogeneous and progressive non-coaxial deformation.

7.2. Original geometries of sheath folding

The original geometry and orientation of buckle folds that subsequently undergo shearing to create sheath folds is frequently difficult to decipher due to the intensity of the ensuing progressive deformation. As noted above, the preservation of NNE-trending fold hinges broadly orthogonal to shear within some lower strain settings clearly suggests that significant hinge rotations have occurred in the higher strain settings where hinges are now sub-parallel to the WNW transport direction. In addition, the reduction in apical angles from the upper to lower limbs of major sheath folds also demonstrates that the preserved apical angle is largely a product of *variable* hinge rotation, rather than *variable* initial buckle fold trends on each major fold limb. Comparison of fold hinge/extension lineation angles with axial planar/foliation angles enables FTPs to be divided into quadrants with clustering of data towards the central intersection reflecting overall greater strain (and rotation) on the lower fold limb (Fig. 10i and m). The absence of any such relationship with lineation parallel fold hinges displaying highly variable axial planar attitudes may suggest that folding *initiated* at variable angles to the transport direction (Fossen and Rykkelid, 1990; Alsop and Holdsworth, 2002). Detailed analysis of geometric relationships on FTPs may thus permit sheath folds generated from a range of original fold orientations varying from either transport-normal to transport-parallel end members to be distinguished (see discussion in Skjernaa, 1989; Fossen and Rykkelid, 1990). In addition, FTPs may also be used to discriminate sheath folds which have undergone significant planar and linear fabric rotations from those transport-parallel folds which are generated either sub-parallel to transport due to existing linear anisotropy (e.g. Watkinson and Cobbold, 1981) or differential shear (e.g. Hansen, 1971; Coward and Potts, 1983; Ridley, 1986; Alsop and Holdsworth, 2002).

The wavelength of fold hinge-line vergence is typically greater for larger folds of thicker units (e.g. Ghosh and Sengupta, 1984), while experimental studies suggest more pronounced non-cylindricity is generated in mechanically heterogeneous materials (Ghosh and Ramberg, 1968; Dubey and Cobbold, 1977). Variable deformation across medial surfaces will to some extent reflect the original orientation of the fold hinge relative to the direction of shear. Greater rotation and strain within the long hinge-line segments may suggest that they were originally orientated at a higher angle to the shear direction than the short hinge-line segments (which suffered less deformation). Consistent discrepancies in the amount and sense of fold hinge-line rotation around medial surfaces are indicative of the original systematic variation in the attitude and obliquity of hinge-lines around the transport direction as may be anticipated in a gently-curvilinear system of 'porpoising' folds (e.g. Wood and Oertal, 1980). S and Z folds displaying different trends on the upper limbs of sheaths have previously been used to define the transport direction via the 'separation arc method' (e.g. Hansen, 1971). However, this study demonstrates that such an arc need not be symmetrically bisected by the transport direction, and may result in significant inaccuracies in calculating transport where broad gaps in data exist. Alternatively, symmetrical hinge-line rotations and fabric relationships on either margin of a medial surface indicate that the extension lineation has acted as an acute bisector of originally symmetrical whaleback folding (see fig. 10 in Alsop and Holdsworth, 1999).

Classical simple-shear generated models of sheath folding, with smooth parabolic hinge-lines defining hair-pin closures, results in extreme hinge elongation defining tubular folds. The X axis of such 'test tube' geometries will display a high ratio when compared with Y–Z axes, and will therefore encourage 'eye-shaped' (Y–Z) sections through the noses of sheaths. Major sheath folds marked by pronounced fold hinge-line vergence may also display acute apical angles and tear-drop eye folds, but need not extend so dramatically in the X-direction owing to mesoscopic reversals in hinge obliquity about the extension lineation (Fig. 14). Such geometries provide an effective means of closing major, kilometre-scale tubular sheaths in which fold hinges are consistently sub-parallel to the extension lineation, and which otherwise may extend for unfeasible distances in the X direction, e.g. a sheath fold with a 1-km-long Y axis and apical angle of 5° (similar to values in Melness) would extend for more than 11 km in the X direction using the simple trigonometry of Lacassin and Mattauer (1985). This problem is further exasperated on overturned limbs where apical angles of tubular folds may be even more acute and dimensions along the X axis become untenable (~30 km!) without recourse to fold hinge-line vergence. Original patterns of mildly curvilinear folding thus provide a fundamental control on the geometric evolution of sheath systems.

7.3. Kinematics of sheath folding

The analysis of sheath fold geometries as an aid to the interpretation of the gross kinematics and determination of shear sense within shear zones has long been discussed. Microstructural studies demonstrate that asymmetric quartz c-axis patterns frequently display an apparent reversal in sense around fold hinges, suggesting that c-axis patterns have been folded around hinges which range from transport-normal (Carreras et al., 1977) to transport-parallel (Shelley and Bossière, 1999). Such reversals suggest a lack of marked fold hinge rotation and recrystallization, which would destroy pre-existing fabrics. However, within sheath folds that have undergone marked hinge rotations, quartz c-axis fabric patterns frequently display the same sense of asymmetry on either limb of the fold (e.g. Carreras et al., 1977; Crispini and Capponi, 1997). This reflects continued dynamic recrystallization during fold hinge rotation associated with progressive non-coaxial deformation.

Important distinctions should be drawn between the bulk kinematics of high strain zones, and localised zones of high strain developed around sheath fold closures in which the local sense of shear reflects variable differential displacement about the fold nose. The relative sense of shear within these enveloping high strain zones may reverse on crossing both axial surfaces and medial surfaces (see e.g. Alsop, 1994). These relationships demonstrate that reversals in shear sense about transport-parallel fold hinges can be generated during a single progressive deformation. They may not therefore simply be a consequence of refolding of pre-existing high strain foliations and shear criteria, and details of fabric overprinting relationships should be carefully examined (see Goscombe and Trouw, 1998).

Several textbooks have recently suggested that sheath folds consistently close in the direction of movement and are therefore of value in determining overall shear sense (e.g. Van der Pluijm and Marshak, 1997, p. 280; Davis and Reynolds, 1996, p. 534; Passchier and Trouw, 1996, p. 124; Twiss and Moores, 1992, p. 63). However, this study clearly demonstrates that both domal and basinal sheath end members that close in opposing directions are generated within the same (top-to-the-west) kinematic regime. The sense of sheath closure is thus governed by the geometry of the original antiformal/synformal buckle folding, coupled with variable amounts and senses of planar and linear fabric rotations between the upper and lower limbs (across the axial surfaces) of major domal and basinal sheath folds. The *direction* of sheath closure is therefore not diagnostic of the *sense* of shear, although clearly the *trend* of movement will bisect the sheath closure (Fig. 2). This study illustrates that sheath folding may only be used to determine the *sense* of shear if the *direction* of sheath closure is combined with the systematic analysis of patterns of fold facing coupled with minor fold and fabric attenuation.

8. Conclusions

1. A suite of seven geometric parameters, which during progressive non-coaxial deformation undergo sequential and ordered modification, may be used to identify regions of lower and higher strain. Detailed analysis of such systematic relationships on FTPs provides a new structural tool that effectively monitors planar and linear fabric rotations and thereby enables a clearer understanding of deformation behaviour. The statistical consistency of our results also allows the predictive methodology developed and tested in this study to be confidently applied in areas with poor exposure and/or fewer data. Such techniques may be applied in all terranes in which heterogeneous deformation results in the rotation of planar and linear structural elements towards the fabric attractor.
2. Distinct strain gradients exist from both the upper and lower limbs of sheath folds which are thus asymmetric across the axial surface, and also from the short hinge-line to long hinge-line segments of sheath folds which are thus asymmetric across the foliation-normal and transport-parallel medial (culmination/depression) surfaces. Major sheath folds may thus be effectively divided into quadrants with different amounts and combinations of planar and linear fabric rotations within each domain, which may be systematically analysed via a *ranking grid.*
3. Axial surfaces of sheath folds are curviplanar about the transport direction. The *sense* of axial plane/foliation obliquity for S and Z folds always remains fixed—no matter what the position relative to medial surfaces, i.e. facing, or position relative to large-scale axial surfaces, i.e. on the lower or upper limbs. However, the acute angle will reduce as strain increases. On stereographic projections, Z and S axial surfaces intersect parallel to L2, thus enabling the transport to be determined in areas where the lineation is absent or ambiguous.
4. Minor fold axial planes show consistent patterns of rotation irrespective of facing, with Z fold axial planes rotating clockwise and S fold axial planes anticlockwise. Minor Z and S fold hinges will display either clockwise or anticlockwise rotation depending on facing direction and position relative to medial surfaces, and may therefore rotate in the same (synthetic) sense or in an opposing (antithetic) sense relative to their axial plane. Lower limbs of domes display synthetic rotations whilst the lower limbs of basins show an antithetic sense, which may be analysed on a *rotation grid*.
5. Bedding-cleavage intersection lineations transect clockwise rotating (north-facing) folds in an anticlockwise sense and anticlockwise rotating (south-facing) folds in a clockwise sense. The sense of transection thus indicates the sense of fold rotation (and hence facing!) and is consistent with patterns of fold rotation around culminations and depressions. In areas devoid of younging evidence, the sense of cleavage transection may thus be used to determine the sense of fold rotation and hence infer the direction of fold facing.
6. Apical angles of sheath folds diminish from the upper limb to the lower limb, and from short hinge-line to long hinge-line segments reflecting greater hinge rotation in these higher strain settings. Analysis of lower strain situations, such as that observed in Sleiteil where *tongue folds* display apical angles of $>70°$, allows the structural evolution of sheath folds to be fully examined and demonstrates that the apical angle may not be symmetrically bisected by the extension lineation in lower strain settings.
7. Higher strain settings (lower fold limbs and long hinge-line segments) are marked by transport sub-parallel folds associated with bi-polar facing patterns, whilst lower strain scenarios are marked by variably orientated fold hinges and a greater distribution arc of facing directions. Patterns of hinge rotation between the upper

and lower fold limbs thus suggest that sheath fold geometries have been generated by increasing rotation of variable transport-normal hinges towards the shear direction.

8. Nested, asymmetric *tear-drop eyes* are developed where pronounced fold hinge-line vergence is associated with variably orientated and non-parallel fold hinges on either side of a medial surface. The sense of offset of the centres to inner and outer non-elliptical rings permits fold limb and fold hinge-line vergence to be deduced. The development of a *vergence grid*, which combines fold limb and fold hinge-line vergence data enables relative strain states to be accurately predicted across both medial surfaces and axial surfaces.

Acknowledgements

Fieldwork for this paper was funded under the NERC-BGS–Academic mapping programme awarded to the University of Durham (Grant F60/G2/36). Subsequent additional funding was provided from the Edinburgh Geological Society, the Carnegie Trust and the Welsh bequest of the University of St. Andrews. We thank Simon Hanmer and an anonymous referee for careful and constructive reviews of the paper.

References

Alsop, G.I., 1992. Progressive deformation and the rotation of contemporary fold axes in the Ballybofey nappe, northwest Ireland. Geological Journal 27, 271–283.

Alsop, G.I., 1994. Relationships between distributed and localised shear in the tectonic evolution of a Caledonian fold and thrust zone, northwest Ireland. Geological Magazine 131, 123–136.

Alsop, G.I., Holdsworth, R.E., 1993. The distribution, geometry and kinematic significance of Caledonian buckle folds in the western Moine Nappe, northwestern Scotland. Geological Magazine 130, 353–362.

Alsop, G.I., Holdsworth, R.E., 1999. Vergence and facing patterns in large-scale sheath folds. Journal of Structural Geology 21, 1335–1349.

Alsop, G.I., Holdsworth, R.E., 2002. The geometry and kinematics of flow perturbation folds. Tectonophysics 350, 99–125.

Alsop, G.I., Holdsworth, R.E., 2004. Shear zone folds: records of flow perturbation or structural inheritance? In: Alsop, G.I., Holdsworth, R.E., McCaffrey, K.J.W., Hand, M. (Eds.) Flow Processes in Faults and Shear Zones. Geological Society Special Publication 224, 177–199.

Alsop, G.I., Holdsworth, R.E., Strachan, R.A., 1996. Transport-parallel cross folds within a mid-crustal Caledonian thrust stack, northern Scotland. Journal of Structural Geology 18, 783–790.

Bell, A.M., 1981. Vergence: an evaluation. Journal of Structural Geology 3, 197–202.

Bell, T.H., 1978. Progressive deformation and reorientation of fold axes in a ductile mylonite zone: the Woodroffe thrust. Tectonophysics 44, 285–321.

Berthé, D., Brun, J.P., 1980. Evolution of folds during progressive shear in the South Amorican Shear Zone, France. Journal of Structural Geology 2, 127–133.

Beunk, F.F., Page, L.M., 2001. Structural evolution of the accretional continental margin of the Paleoproterozoic Svecofennian orogen in southern Sweden. Tectonophysics 339, 67–92.

Boettcher, S.S., Mosher, S., 1998. Mid- to late-ductile deformation and thermal evolution of the crust in the northern Dome Rock Mountains, Arizona. Journal of Structural Geology 20, 745–764.

British Geological Survey, 1997. Tongue, Scotland 114E. Solid Geology. 1:50,000.

British Geological Survey, 2002. Loch Eriboll, Scotland 114W. Solid Geology. 1:50,000.

Carey, S.W., 1962. Folding. Journal of the Alberta Society of Petroleum Geology 10, 95–144.

Carreras, J., Estrada, A., White, S., 1977. The effect of folding on the c-axis fabrics of a quartz mylonite. Tectonophysics 39, 3–24.

Cobbold, P.R., Quinquis, H., 1980. Development of sheath folds in shear regimes. Journal of Structural Geology 2, 119–126.

Coward, M.P., Potts, G.J., 1983. Complex strain patterns developed at the frontal and lateral tips to shear zones and thrust zones. Journal of Structural Geology 5, 383–399.

Crispini, L., Capponi, G., 1997. Quartz fabric and strain partitioning in sheath folds: an example from the Voltri Group (Western Alps, Italy). Journal of Structural Geology 19, 1149–1157.

Davis, G.H., Reynolds, S.J., 1996. Structural Geology of Rocks and Regions, 2nd Ed, Wiley, New York.

Davison, I., Bosence, D., Alsop, G.I., Al-Aawah, M.H., 1996. Deformation and sedimentation around active Miocene salt diapirs on the Tihama Plain, northwest Yemen. In: Alsop, G.I., Blundell, D.J., Davison, I. (Eds.), Salt Tectonics. Geological Society of London Special Publication 100, pp. 23–39.

D'el-Roy Silva, L.J.H., Barros Neto, L.S., 2002. The Santa Terezinha–Campos Verdes emerald district, central Brazil: structural and Sm–Nd data to constrain the tectonic evolution of the Neoproterozoic Brasília belt. Journal of South American Earth Sciences 15, 693–708.

Dubey, A.K., Cobbold, P.R., 1977. Noncylindrical flexural slip folds in nature and experiment. Tectonophysics 38, 223–239.

Escher, A., Watterson, J., 1974. Stretching fabrics, folds and crustal shortening. Tectonophysics 22, 223–231.

Ez, V., 2000. When shearing is a cause of folding. Earth Science Reviews 51, 155–172.

Fletcher, J.M., Bartley, J.M., 1994. Constrictional strain in a non-coaxial shear zone: implications for fold and rock fabric development, central Mojave metamorphic core complex, California. Journal of Structural Geology 16, 555–570.

Fletcher, J.M., Bartley, J.M., Martin, M.W., Glazner, A.F., Walker, J.D., 1995. Large-magnitude continental extension, an example from the central Mojave metamorphic core complex. Geological Society of America Bulletin 107, 1468–1483.

Fossen, H., Rykkelid, E., 1990. Shear zone structures in the Øygarden area, West Norway. Tectonophysics 174, 385–397.

Ghosh, S.K., Ramberg, H., 1968. Buckling experiments on intersecting fold patterns. Tectonophysics 5, 89–105.

Ghosh, S.K., Sengupta, S., 1984. Successive development of plane noncylindrical folds in progressive deformation. Journal of Structural Geology 6, 703–709.

Ghosh, S.K., Hazra, S., Sengupta, S., 1999. Planar, non-planar and refolded sheath folds in the Phulad Shear Zone, Rajasthan, India. Journal of Structural Geology 21, 1715–1729.

Goscombe, B., 1991. Intense non-coaxial shear and the development of mega-scale sheath folds in the Arunta Block, Central Australia. Journal of Structural Geology 13, 299–318.

Goscombe, B.D., Trouw, R., 1998. The geometry of folded tectonic shear sense indicators—an assessment from field data. Journal of Structural Geology 25, 575–589.

Hanmer, S., Greene, D.C., 2002. A modern structural regime in the Paleoarchean (~3.64 Ga); Isua Greenstone Belt, southern West Greenland. Tectonophysics 346, 201–222.

Hansen, E., 1971. Strain Facies, Springer-Verlag, New York.

Henderson, J.R., 1981. Structural analysis of sheath folds with horizontal X-axes, northeast Canada. Journal of Structural Geology 3, 203–210.

Hobbs, B.E., Means, W.D., Williams, P.F., 1976. An Outline of Structural Geology, John Wiley and Sons, New York.

Holdsworth, R.E., 1988. The stereographic analysis of facing. Journal of Structural Geology 10, 219–223.

Holdsworth, R.E., 1989. The geology and structural evolution of a Caledonian fold and ductile thrust zone, Kyle of Tongue region, Sutherland, N. Scotland. Journal of the Geological Society of London 146, 809–823.

Holdsworth, R.E., 1990. Progressive deformation structures associated with ductile thrusts in the Moine Nappe, Sutherland, N. Scotland. Journal of Structural Geology 12, 443–452.

Holdsworth, R.E., Grant, C.J., 1990. Convergence-related 'dynamic spreading' in a mid-crustal ductile thrust zone: a possible orogenic wedge model. In: Knipe, R.J., Rutter, E.H. (Eds.), Deformation Mechanisms, Rheology and Tectonics. Geological Society of London Special Publication 54, pp. 491–500.

Holdsworth, R.E., Roberts, A.M., 1984. A study of early curvilinear fold structures and strain in the Moine of the Glen Garry region, Invernessshire. Journal of the Geological Society of London 141, 327–338.

Holdsworth, R.E., Strachan, R.A., Alsop, G.I., 2001. Geology of the Tongue District. Memoirs of the British Geological Survey. Sheet 114E (Scotland), 76pp.

Hudleston, P.J., 1986. Extracting information from folds in rocks. Journal of Geological Education 34, 237–245.

Hudleston, P.J., 1992. A comparison between glacial movement and thrust sheet or nappe emplacement and associated structures. In: Mitra, S., Fischer, G.W. (Eds.), Structural Geology of Fold and Thrust Belts, Johns Hopkins University Press, Baltimore, pp. 81–91.

Jiang, D., Williams, P.F., 1999. When do dragfolds not develop into sheath folds in shear zones? Journal of Structural Geology 21, 577–583.

Lacassin, R., Mattauer, M., 1985. Kilometre-scale sheath fold at Mattmark and implications for transport directions in the Alps. Nature 315, 739–742.

Mies, J.W., 1991. Planar dispersion of folds in ductile shear zones and kinematic interpretation of fold hinge girdles. Journal of Structural Geology 13, 281–297.

Mies, J.W., 1993. Structural analysis of sheath folds in the Sylacauga Marble Group, Talladega slate belt, southern Appalachians. Journal of Structural Geology 15, 983–993.

Minnigh, L.D., 1979. Structural analysis of sheath-folds in a meta-chert from the Western Italian Alps. Journal of Structural Geology 1, 275–282.

Park, A.F., 1988. Geometry of sheath folds and related fabrics at the Luikonlahti mine, Svecokarelides, eastern Finland. Journal of Structural Geology 10, 487–498.

Passchier, C.W., 1997. The fabric attractor. Journal of Structural Geology 19, 113–127.

Passchier, C.W., Trouw, R.A.J., 1996. Microtectonics, Springer-Verlag, Berlin.

Platt, J.P., 1982. Emplacement of a fold-nappe, Betic Orogen, southern Spain. Geology 10, 97–102.

Quinquis, H., Audren, C., Brun, J.P., Cobbold, P.R., 1978. Intense progressive shear in Ille de Groix blueschists and compatibility with subduction or obduction. Nature 273, 43–45.

Ramsay, J.G., 1960. The deformation of early linear structures in areas of repeated folding. Journal of Geology 68, 75–93.

Ramsay, J.G., 1967. Folding and Fracturing of Rocks, McGraw-Hill.

Ramsay, J.G., 1980. Shear zone geometry: a review. Journal of Structural Geology 2, 83–99.

Ramsay, J.G., Huber, M., 1987. The Techniques of Modern Structural Geology. Volume 2: Folds and Fractures, Academic Press, London.

Ramsay, J.G., Lisle, R.J., 2000. The Techniques of Modern Structural Geology. Volume 3: Applications of Continuum Mechanics in Structural Geology, Academic Press, London.

Rhodes, S., Gayer, R.A., 1977. Non-cylindrical folds, linear structures in the X-direction and mylonite developed during translation of the Caledonian Kalak Nappe Complex of Finnmark. Geological Magazine 114, 329–341.

Ridley, J., 1986. Parallel stretching lineations and fold axes oblique to displacement direction—a model and observations. Journal of Structural Geology 8, 647–654.

Roberts, A., 1989. Fold and thrust structures in the Kintradwell "Boulder beds", Moray Firth. Scottish Journal of Geology 25, 173–186.

Sanderson, D.J., 1973. The development of fold axes oblique to the regional trend. Tectonophysics 16, 55–70.

Shelley, D., Bossière, G., 1999. Ile de Groix: retrogression and structural developments in an extensional régime. Journal of Structural Geology 21, 1441–1455.

Skjernaa, L., 1980. Rotation and deformation of randomly oriented planar and linear structures in progressive simple shear. Journal of Structural Geology 2, 101–109.

Skjernaa, L., 1989. Tubular folds and sheath folds: definitions and conceptual models for their development with examples from the Grapesvare area, northern Sweden. Journal of Structural Geology 11, 689–703.

Talbot, C.J., 1979. Fold trains in a glacier of salt in southern Iran. Journal of Structural Geology 1, 5–18.

Twiss, R.J., Moores, E.M., 1992. Structural Geology, Freeman, New York.

Van der Pluijm, B.A., Marshak, S., 1997. Earth Structure: An Introduction to Structural Geology and Tectonics, WCB/McGraw-Hill, Dubuque, Iowa.

Van der Wateren, F., Kluiving, S.J., Bartek, L.R., 2000. Kinematic indicators of subglacial shearing. In: Maltman, A.J., Hubbard, B., Hambrey, M.J. (Eds.), Deformation of Glacial Materials. Geological Society of London Special Publication 176, pp. 259–278.

Velaj, T., Davison, I., Serjani, A., Alsop, G.I., 1999. Thrust tectonics and the role of evaporites in the Ionian Zone of the Albanides. American Association of Petroleum Geologists Bulletin 83, 1408–1425.

Vollmer, F.W., 1988. A computer model of sheath-nappes formed during crustal shear in the Western Gneiss Region, central Norwegian Caledonides. Journal of Structural Geology 10, 735–743.

Watkinson, A.J., Cobbold, P.R., 1981. Axial directions of folds in rocks with linear/planar fabrics. Journal of Structural Geology 3, 211–217.

Williams, G.D., 1978. Rotation of contemporary folds into the X direction during overthrust processes in Laksefjord, Finnmark. Tectonophysics 48, 29–40.

Williams, G.D., Chapman, T.J., 1979. The geometrical classification of noncylindrical folds. Journal of Structural Geology 1, 181–185.

Wood, D.S., Oertal, G., 1980. Deformation in the Cambrian slate belt of Wales. Journal of Geology 88, 285–308.